Imaging surface spots from space photometry

A.F. Lanza
INAF-Osservatorio Astrofisico di Catania, Italy
nuccio.lanza@oact.inaf.it

Besançon, 12 May 2014 – The Surface Cartography of the Sun and the Stars

Solar activity

- In the Sun we can study stellar activity in detail, thanks to the spatial and time resolution (down to 50-100 km and a fraction of a second, respectively);
- In the photosphere, the features associated with magnetic fields are sunspots, faculae, and the network.

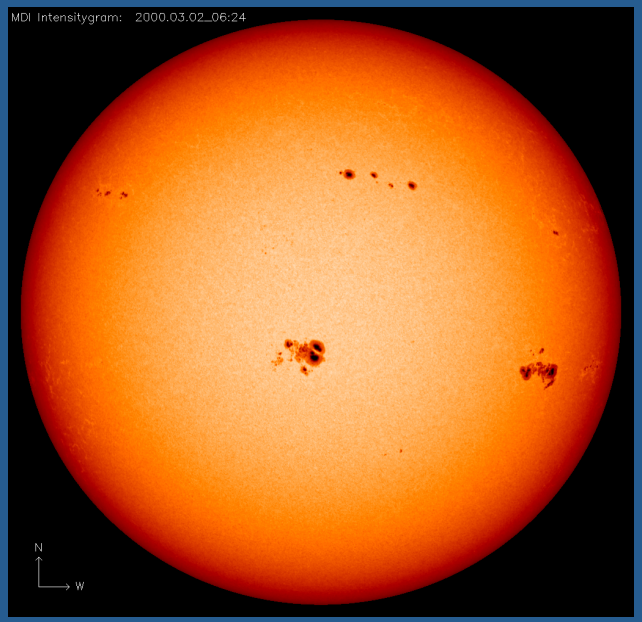

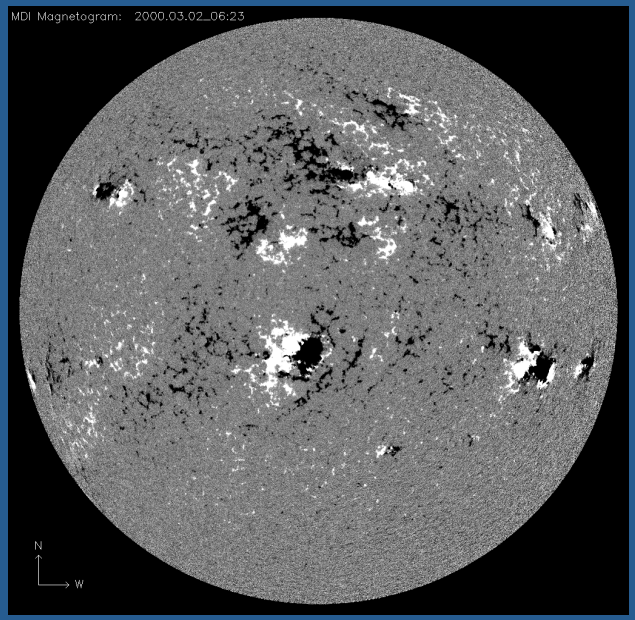

Variation of Solar Irradiances

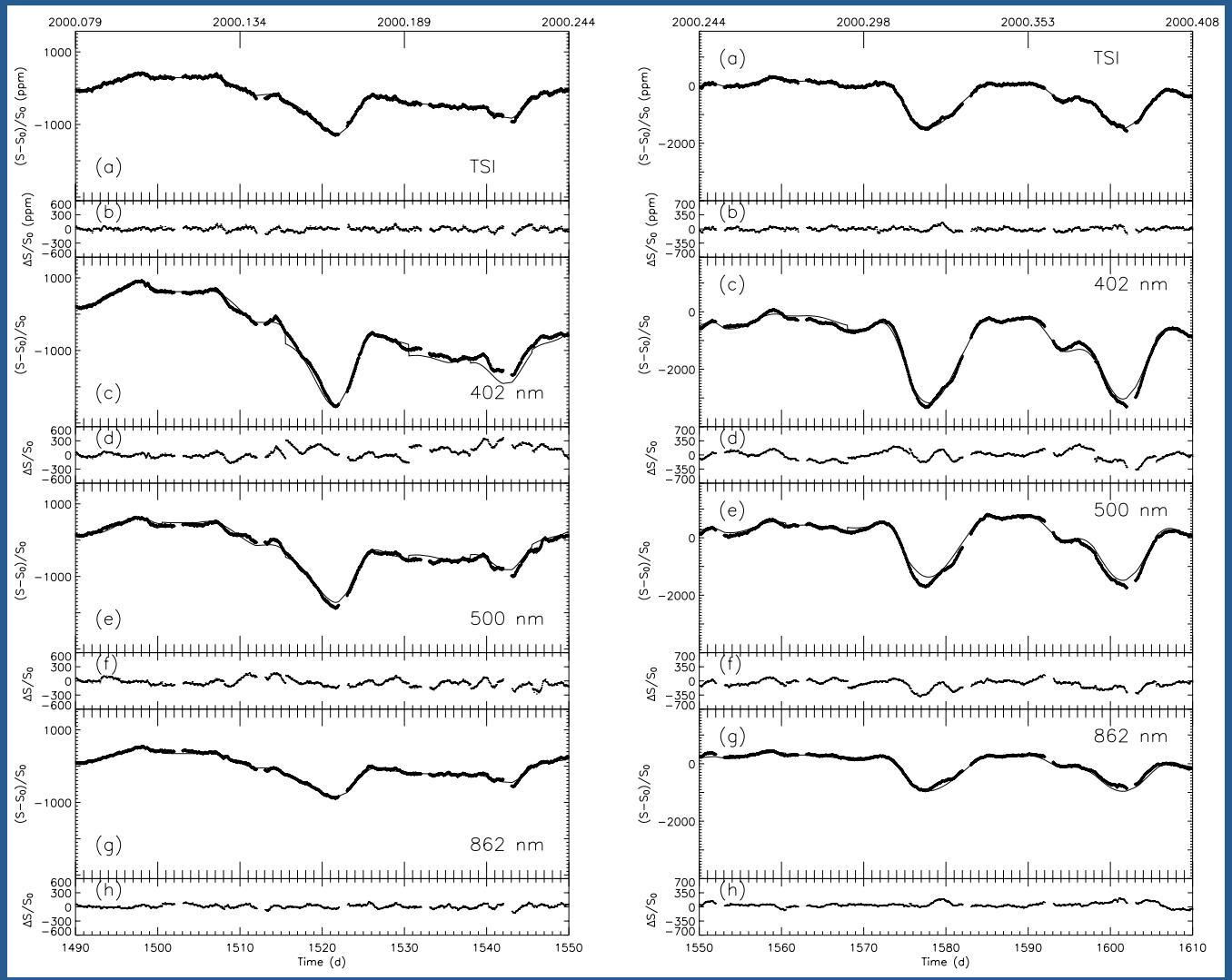

(Lanza et al. 2004)

Photometric effects of an active region

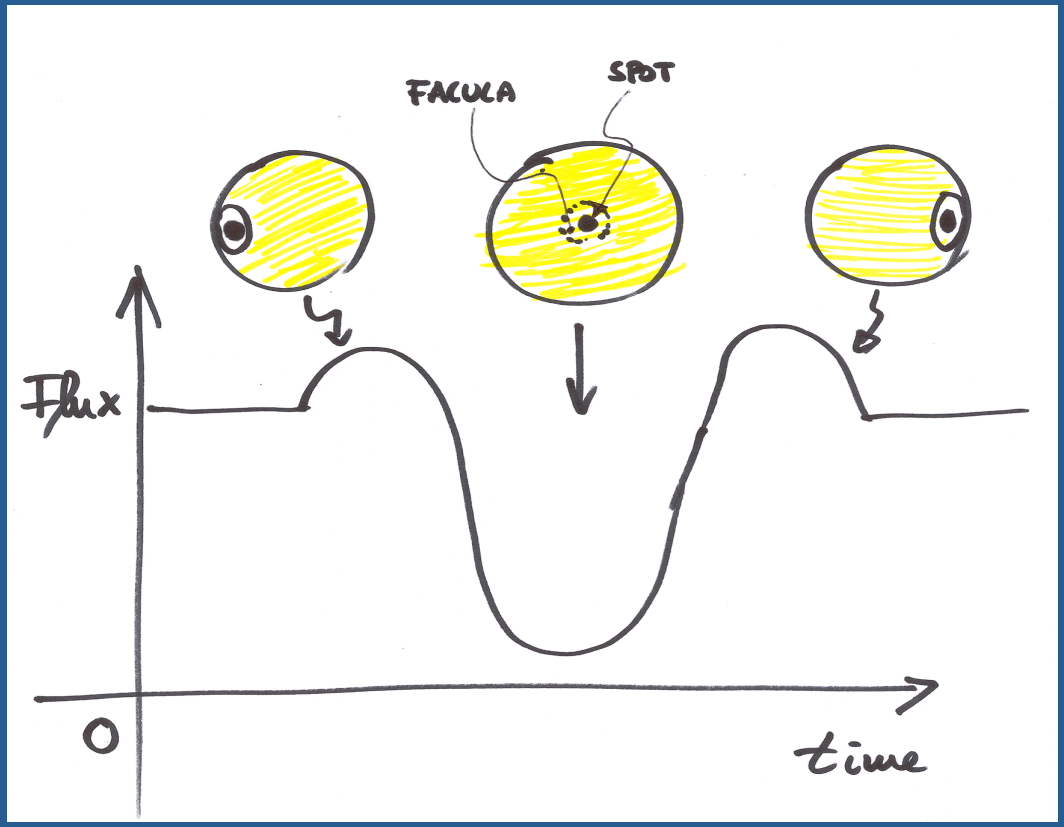

Faculae are more contrasted close to the limb and produce an increase of the flux, while spots produce the maximum flux decrement when they are closer to disc centre because of projection effects. On the other hand, faculae have a small contrast at disc centre, so the effect of the spots is prevailing there.

Stellar activity

- The disks of distant stars cannot generally be resolved (see, however, lectures by Perrin, Kervella, Monnier et al. at this meeting);
- We apply indirect techniques to map their photospheres:
  - Doppler imaging (v sin i ≥ 10-15 km/s is required); see, e.g., Kochukhov (this meeting), Donati & Collier Cameron (1997), Strassmeier (2009; 2011);
  - Modelling of the rotational modulation of the optical flux, i.e, spot modelling (e.g., Lanza et al. 2007);
  - Eclipse mapping in close binary systems (e.g., Collier Cameron 1997; Lanza et al. 1998);
  - Transit mapping in star-planet systems (e.g., Schneider 2000; Silva 2003);
- A general introduction to starspot activity in late-type stars can be found in, e.g., Berdyugina (2005) and Strassmeier (2009).

Space-borne photometry

- Thanks to space-borne photometric experiments (MOST, CoRoT, and Kepler) high-precision (20-300 ppm for 1 hr integration time on a V=12 G2V star) and uninterrupted (up to 150-1200 days) optical photometric time series are now available to map stellar photospheres;

- Those time-series were primarily acquired to search for planetary transits;

- If a transit is discovered, this leads to complementary and follow-up observations that allow us a full characterization of the star;

- The out-of-transit time series can then be used to study stellar activity and relate its characteristics to stellar parameters.

Time-series analysis

- Several approaches based on different methods for time series analysis have been proposed and applied to stellar light curves to derive:
  - Rotation periods and differential rotation;
  - Spot lifetimes;
  - Active longitudes;
  - Activity cycles;
- see, e.g., Jetsu (1996); Donahue et al. (1997), Kollath & Olah (2009); Lehtinen et al. (2011); Lindborg et al. (2013); McQuillan et al. (2013, 2014); Walkowitz & Basri (2013); Reinhold et al. (2013);
- Here, we shall focus on spot modelling and do not consider further those approaches.

Principles of spot modelling

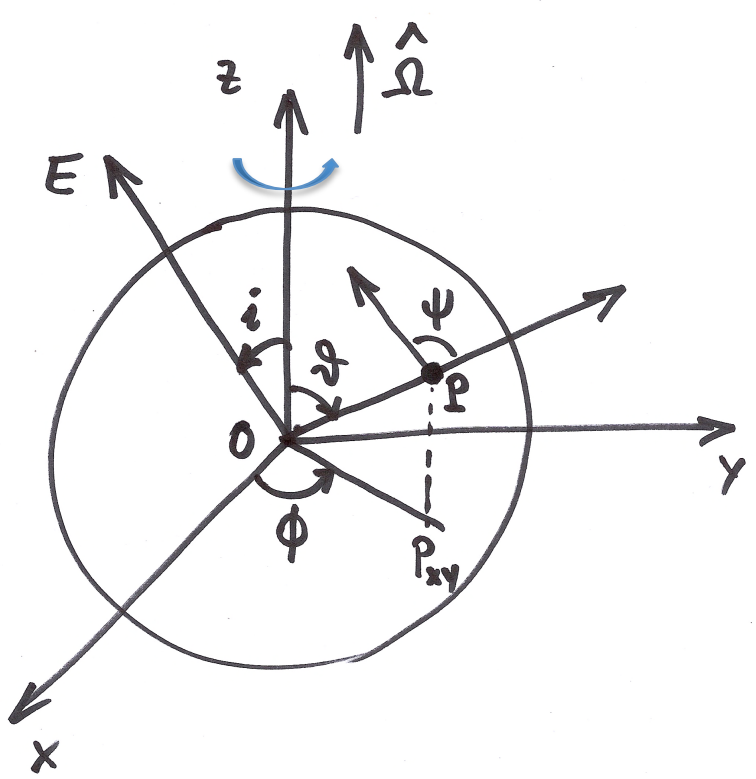

We consider a Cartesian reference frame in which the Z-axis is directed along the spin axis of the star while the X and Y axes are fixed in an inertial space. The X-axis is chosen so that the line of sight to the observer OE is contained in the XZ plane.

θ is the colatitude of the point P on the surface of the star, ϕ its longitude, i the inclination of the stellar spin axis to the line of sight, and ψ is the angle between the normal to the surface element and the line of sight.

If Ω is the angular velocity of rotation of the star:

$$\phi(t) = \phi_0 + \Omega(t - t_0), \tag{1}$$

where ϕ_0 is the initial longitude at the initial time t_0, and t is the time. Then we have:

$$\begin{aligned} \hat{OE} &= (\sin i,\ 0,\ \cos i) \\ \hat{OP} &= (\sin\theta\cos\phi(t),\ \sin\theta\sin\phi(t),\ \cos\theta) \\ \mu \equiv \cos\psi &= \hat{OE}\cdot\hat{OP} = \sin i\sin\theta\cos\phi(t) + \cos i\cos\theta \end{aligned} \tag{2}$$

$$\mu = \sin i\sin\theta\cos\left[\phi_0 + \Omega(t - t_0)\right] + \cos i\cos\theta \tag{3}$$

Estimating stellar inclination

- The photometric period P_{rot}, derived from the light modulation induced by starspots, can be combined with the measurement of the *v*sin*i* and an estimate of the stellar radius *R* to derive the inclination:

$$\sin i = P_{rot}\,(v \sin i) \,/\, (2\pi R)$$

- Asteroseismology can also provide a measure of the inclination (e.g., Gizon & Solanki 2003; Ballot et al. 2006, 2011).

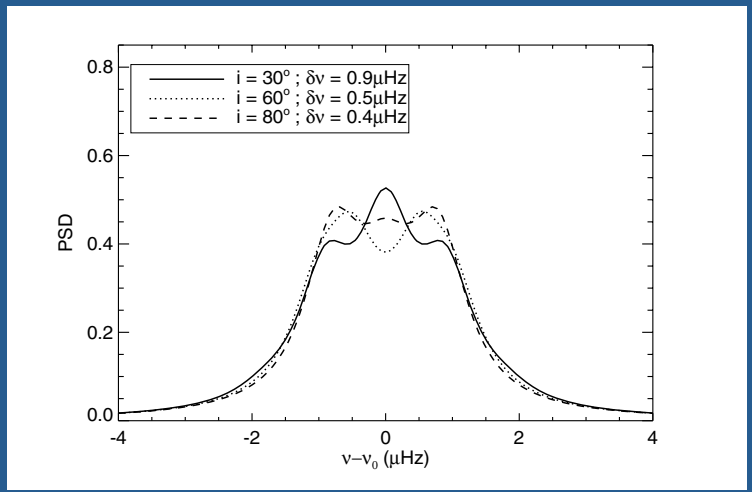

(Ballot et al. 2006)

Specific intensity and flux

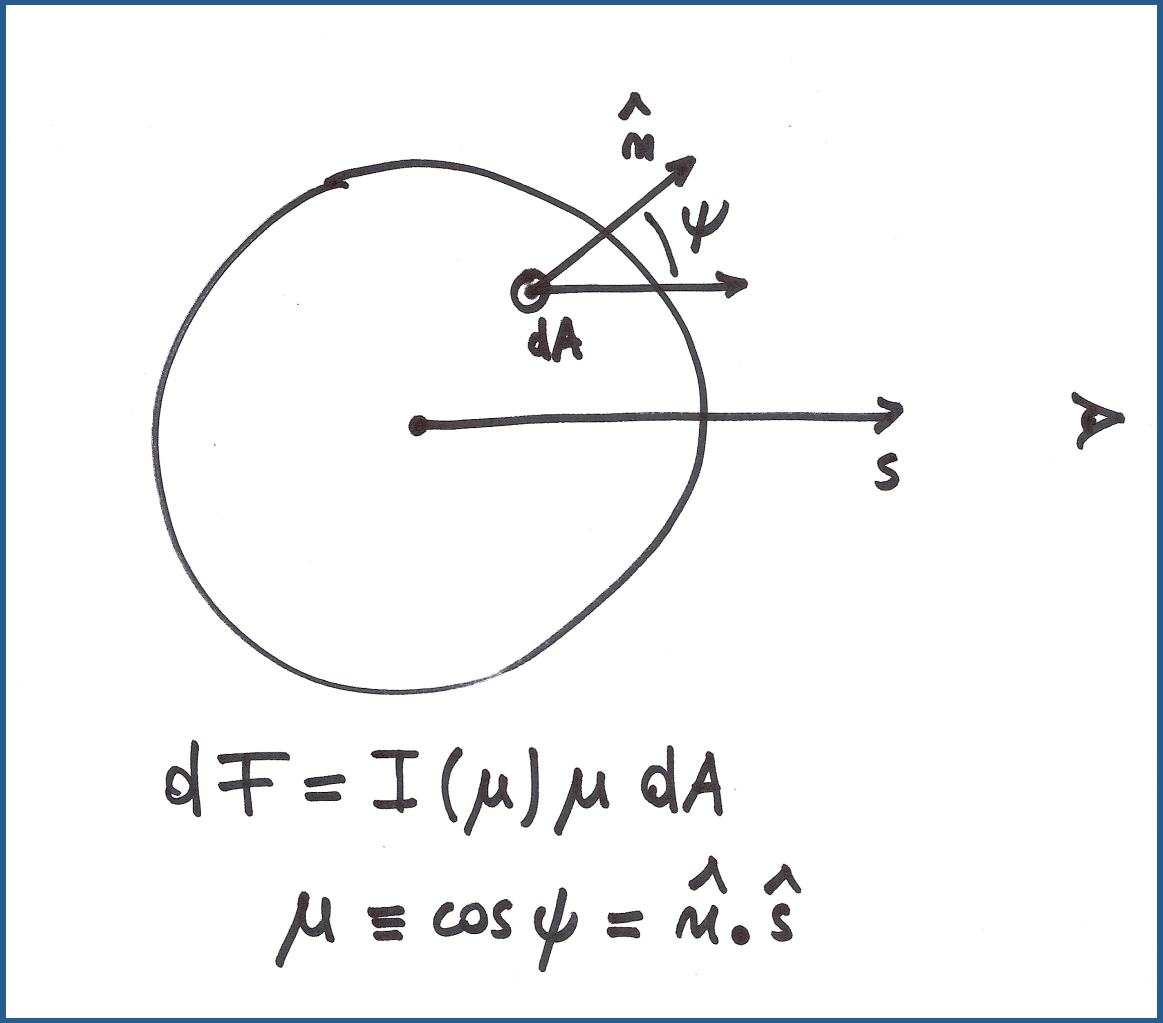

Let us assume a quadratic limb-darkening law for the unperturbed photosphere in the given passband:

$$I_{\rm u}(\mu) = I_0(a + b\mu + c\mu^2), \tag{4}$$

where $I_{\rm u}$ is the specific intensity in the given passband, I_0 is the specific intensity at the centre of the disc, a, b, and c are the limb-darkening coefficients that verify $a + b + c = 1$, and $\mu \equiv \cos\psi$.

The total flux coming from the stellar disc of radius R is:

$$F_{\rm u} = 2\pi R^2 \int_0^{\pi/2} I_{\rm u}(\cos\psi)\cos\psi\sin\psi\, d\psi = 2\pi R^2 \int_0^1 I_{\rm u}(\mu)\mu\, d\mu$$

$$F_{\rm u} = \pi R^2 I_0 \left(a + \frac{2}{3}b + \frac{1}{2}c\right). \tag{5}$$

The flux perturbation produced by dark spots and bright faculae contained within a small surface element centred around the point P is:

$$\Delta F = \Delta F_{\rm s} + \Delta F_{\rm f} = A_{\rm s}\mu(I_{\rm s} - I_{\rm u}) + A_{\rm f}\mu(I_{\rm f} - I_{\rm u}),$$

where $A_{\rm s}$ is the area of the spots and $A_{\rm f}$ that of the faculae.

If A is the area of the surface element, we define the filling factor of the spots $f_{\rm s}$ and that of the faculae Qf according to:

$$A_{\rm s} = f_{\rm s}A, \quad A_{\rm f} = Qf_{\rm s}A = QA_{\rm s},$$

and their intensity contrasts as:

$$c_{\rm s} \equiv \left(1 - \frac{I_{\rm s}}{I_{\rm u}}\right), \quad c_{\rm f} \equiv -\left(1 - \frac{I_{\rm f}}{I_{\rm u}}\right).$$

Solar faculae are more contrasted toward the limb and virtually invisible at disc centre; therefore, we assume:

$$c_{\rm f} = c_{\rm f0}(1 - \mu),$$

so that

$$\Delta F = A_{\rm s}I_{\rm u}(\mu)\left[-c_{\rm s} + Qc_{\rm f0}(1-\mu)\right]\mu = f_{\rm s}A\, I_{\rm u}(\mu)\left[-c_{\rm s} + Qc_{\rm f0}(1-\mu)\right]\mu. \tag{6}$$

In addition, to further simplify our model, we assume that:

a) the star is spherically symmetric – a rotationally or tidally distorted star shows gravity darkening in addition to limb darkening, thus complicating the model;

b) the contrasts $c_{\rm s}$ and c_{f0} are constant;

c) the ratio of the facular-to-spotted area $Q \equiv A_{\rm f}/A_{\rm s}$ is constant;

d) the presence of spot penumbra is neglected;

e) active regions are assumed to be point-like to compute projection effects ($A_{\rm s},\ A_{\rm f} \ll \pi R^2$).

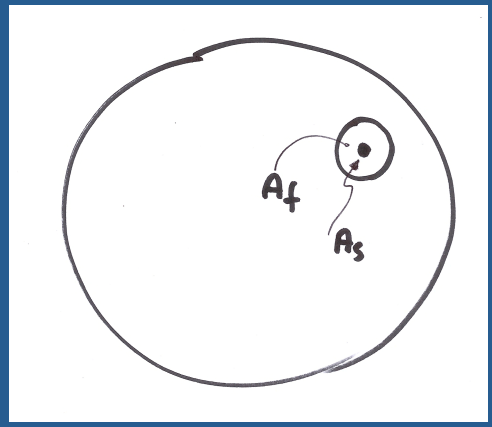

Effect of a single active region

We assume that a given active region consists of spots of area A_s and faculae of area $A_\mathrm{f} = QA_\mathrm{s}$ localized into a given surface element with central coordinates (θ, ϕ_0).

The observed flux at the time t is:

$$F(t) = F_\mathrm{u} + \Delta F(t)$$

and its relative variation, according to Eq. (6):

$$\frac{F(t)}{F_\mathrm{u}} = 1 + \frac{\Delta F(t)}{F_\mathrm{u}} = 1 + \frac{A_\mathrm{s} I_\mathrm{u}(\mu)}{F_\mathrm{u}} \left[Qc_\mathrm{f0}(1-\mu) - c_\mathrm{s}\right] v(\mu)\mu, \tag{7}$$

or, substituting Eqs. (4) and (5) into Eq. (7):

$$\frac{F(t)}{F_\mathrm{u}} = 1 + \left(\frac{A_\mathrm{s}}{\pi R^2}\right)\left(\frac{a + b\mu + c\mu^2}{a + 2b/3 + c/2}\right) \left[Qc_\mathrm{f0}(1-\mu) - c_\mathrm{s}\right] v(\mu)\mu, \tag{8}$$

where the time dependence comes through μ:

$$\mu = \sin i \sin\theta \cos\left[\phi_0 + \Omega(t - t_0)\right] + \cos i \cos\theta,$$

and v is the *visibility* of the surface element defined as:

$$v(\mu) = \begin{cases} 1 & \text{if } \mu \geq 0 \\ 0 & \text{if } \mu < 0. \end{cases}$$

Extended polar-cap spots

- Polar cap spots have been considered in the case of very active stars because spots cover a significant fraction of the stellar disc;
- They were quite popular in the ‘80 and ‘90 to fit ground-based photometry;
- Dorren (1987) and Eker (1994), among others, provided the theory of their light variation.

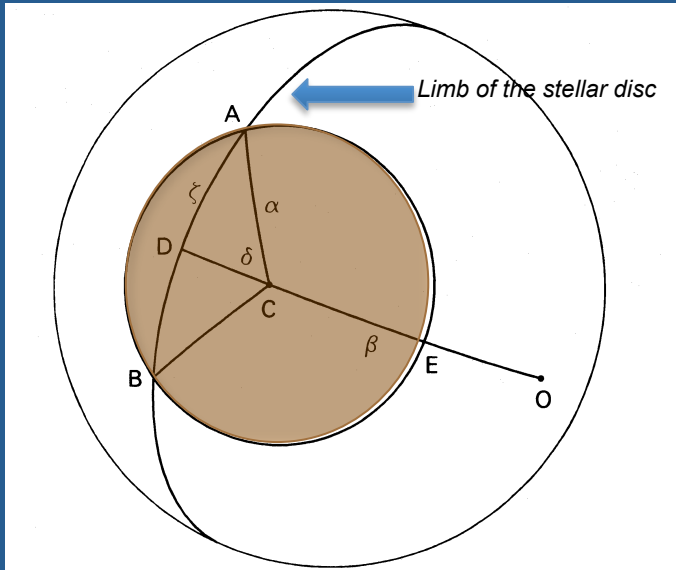

FIG. 1.—Geometry of a partly visible spot. O is the center of the visible hemisphere, which is intersected by the spot at A and B. The great circle through O and the spot center C intersects the spot at E, and the edge of the visible hemisphere at D. $OC = \beta$, $ACD = \delta$, $AD = \zeta$, $ADC = \pi/2$, and $AC = \alpha$, the spot radius.

Few-spot models

- We can model the light curve of an active star by considering the simultaneous effects of 2-3 non-overlapping spots;
- It is sufficient to add the effects of the single spots as described in the previous slides;
- When we consider 2 spots, the free parameters are:
  - Stellar parameters: inclination i, $P_{rot} = 2\pi/\Omega$, limb-darkening coefficients;
  - The unspotted flux level F_u (usually assumed equal to the maximum of the light curve or specified as a constant);
  - The spot and facular contrasts, c_s and c_{f0}, respectively, and the ratio of the facular-to-spotted area Q;
  - For each spot: relative area $A_s/\pi R^2$, colatitude θ, initial longitude ϕ_0 (spot geometric parameters).
- By fixing i, P_{rot}, F_u, Q, the contrasts and the limb-darkening coefficients, we search for the 6 spot geometrical parameters that minimize the χ^2 of the fit to the observations;

2-spot modelling

- The model can be unique only because of the small number of free parameters;
- In general, there are several degeneracies among the parameters (e.g., i vs. θ);
- It was acceptable for ground-based photometry with a precision of 0.01-0.02 mag, but its residuals are too large for space-borne photometry for which a typical precision is 10^{-4} mag;
- Increasing the number of spots makes the residuals smaller, but the degeneracies among parameters become much stronger and the solution highly non-unique leading to an unstable best fit;
- For specific applications, 2-spot models in combination with a Monte Carlo Markov Chain approach to sample the parameter space are useful, e.g., to estimate differential rotation (Croll 2006; Lanza et al. 2014).

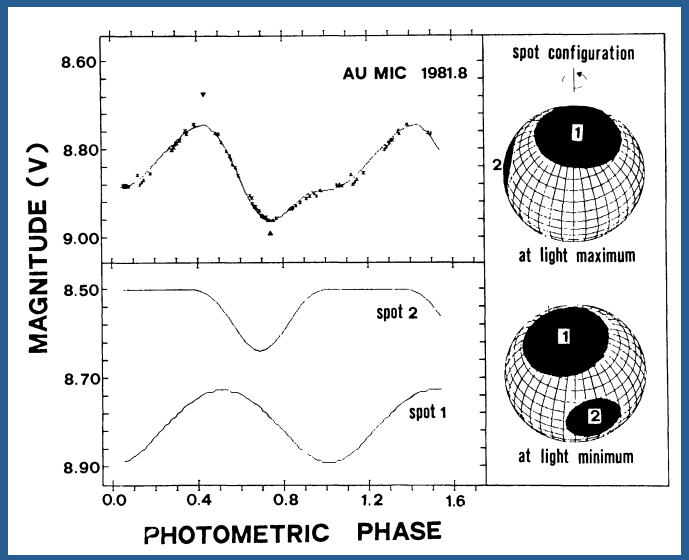

(Rodonò et al. 1986)

Two-spot model of ε Eridani

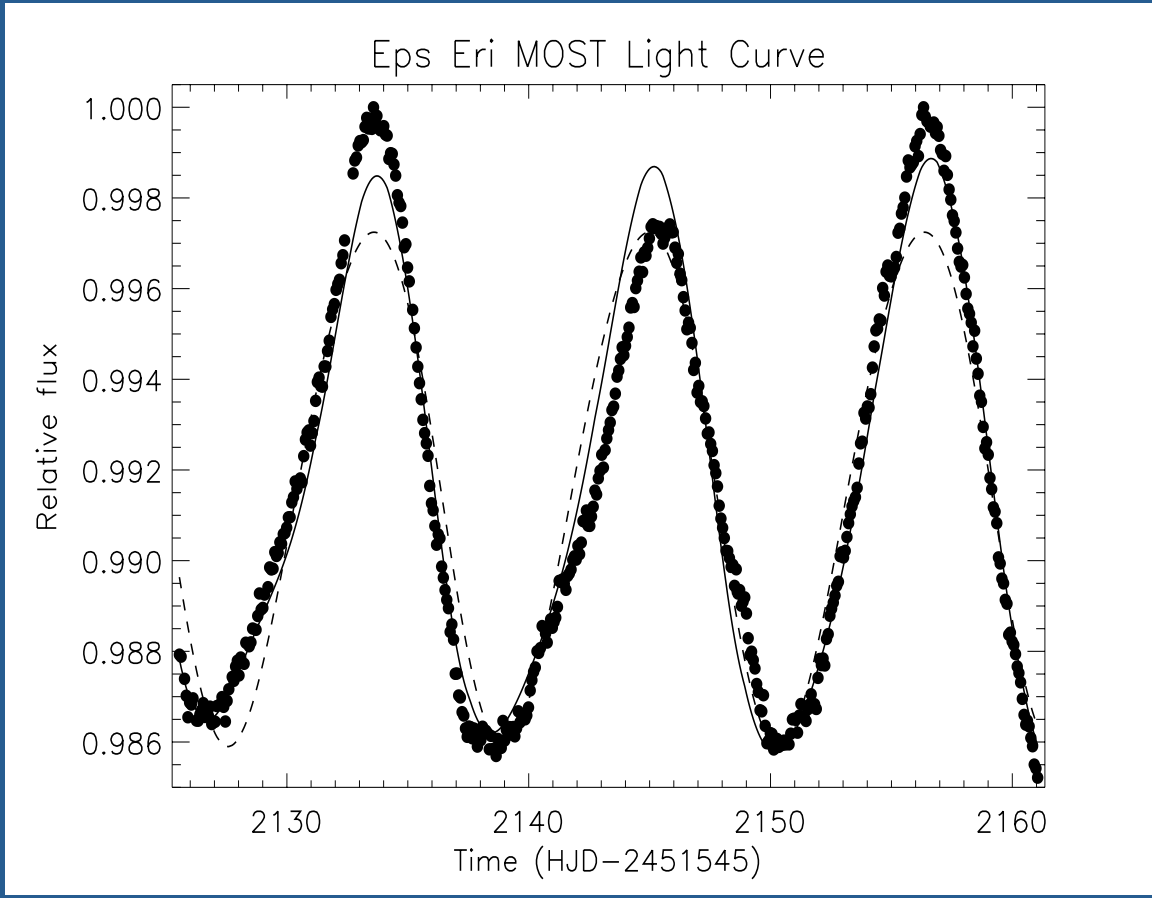

MOST light curve (filled dots) fitted with a 2-spot model with differential rotation (solid line) and with rigid rotation (dashed line) (Croll et al. 2006; Croll 2006; Lanza et al. 2014).

The facular-to-spotted area ratio

CoRoT-2 (Lanza et al. 2009a)

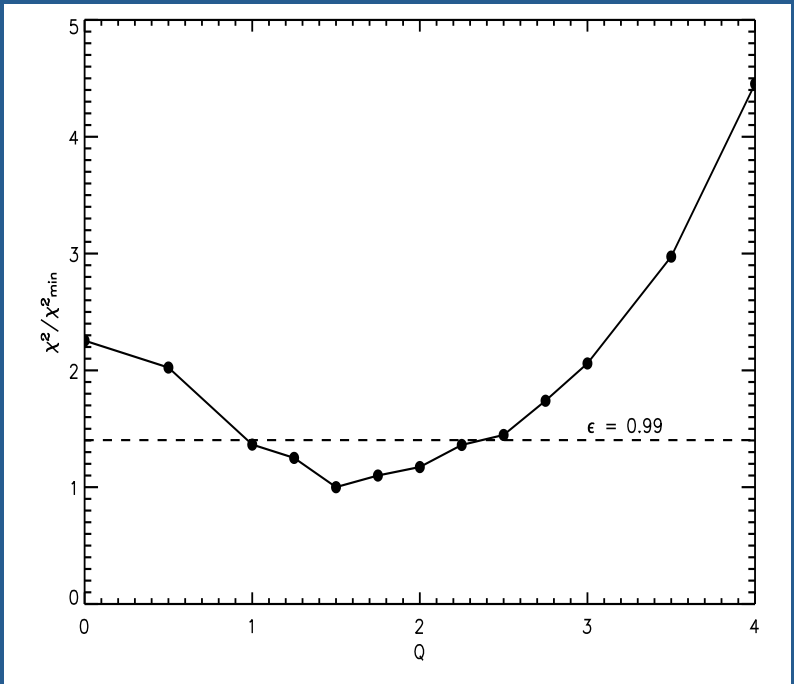

Kepler-17 (Bonomo & Lanza 2012)

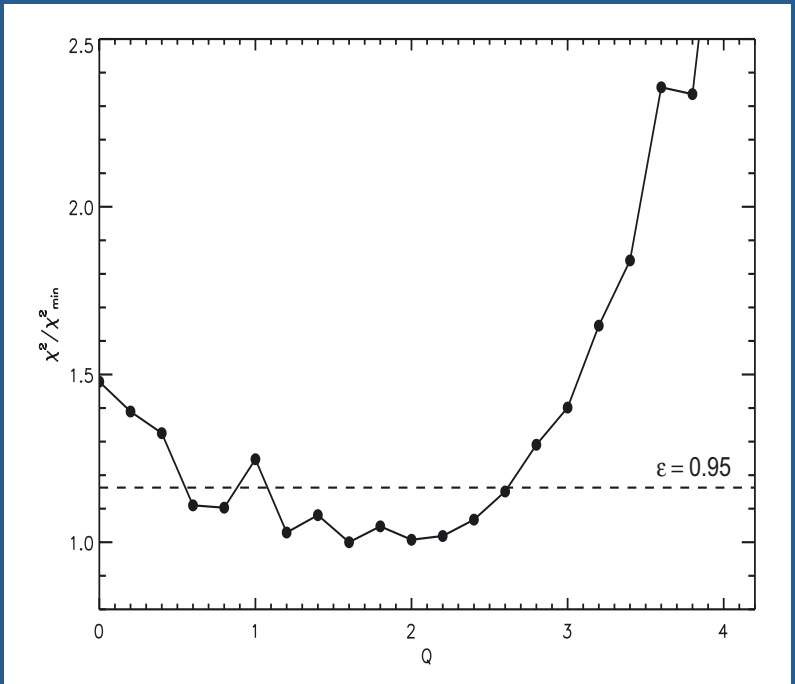

- Few-spot models may be used to estimate *Q* by minimizing the χ^2 vs. that parameter.

Multi-spot models with evolution

- Mosser et al. (2009) fitted the light curves of several CoRoT asteroseismic targets using a model with evolving spots;
- During each rotation, 2-3 spots were assumed;
- Solutions are obtained by a relaxed χ^2 minimization using a technique similar to simulated annealing;
- The method was extensively tested with simulated data to study the dependence of the results on the model assumptions and the parameters held fixed;
- The model proved useful to derive:
  - Spot lifetimes;
  - Mean rotation period;
  - Other parameters could also be derived, but with a sensible dependence on model assumptions:
    - Inclination of the spin axis;
    - Spot latitudes;
    - Latitudinal differential rotation.

Spot latitudes from transit times

- The information on the latitudes of individual spots comes from their transit times across the stellar disc, in the case of a star not viewed equator-on;
- However, even in the case of a single spot, latitude is largely degenerate with the inclination of the stellar spin axis;
- Surface differential rotation can affect the result;
- In the case of a model with several spots, their latitudes are generally ill-defined and depend on model assumptions and fixed parameters.

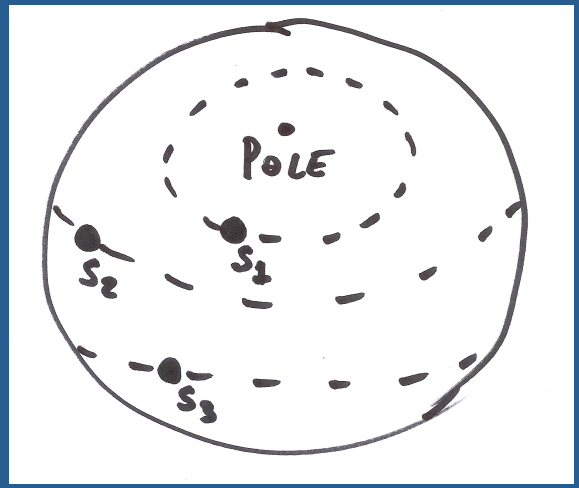

Bayesian multi-spot modelling

- Fröhlich (2007), Frasca et al. (2011), and Fröhlich et al. (2012) proposed models with several discrete spots based on a Bayesian estimate of the spot and stellar parameters using Monte Carlo Markov Chains.

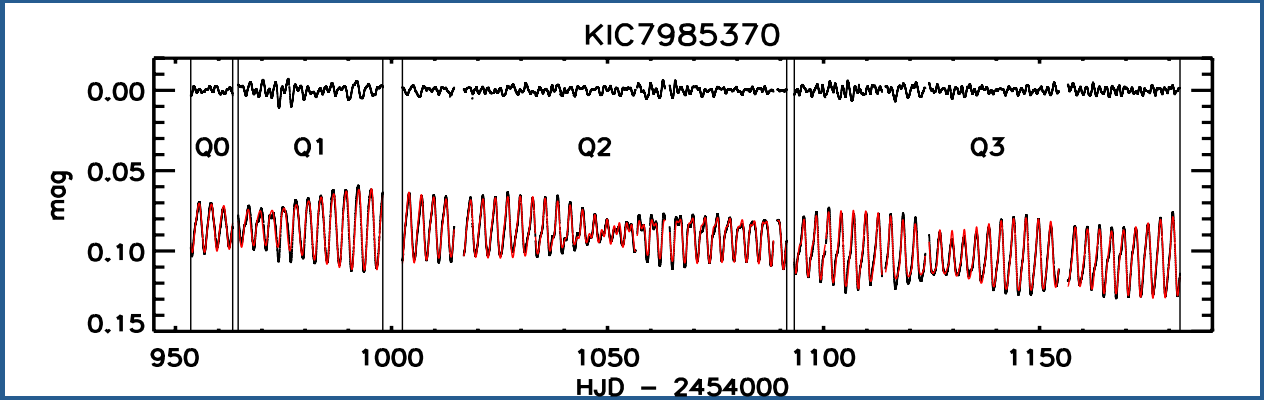

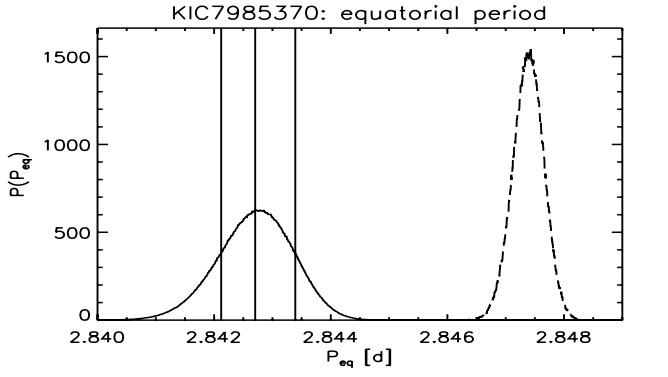

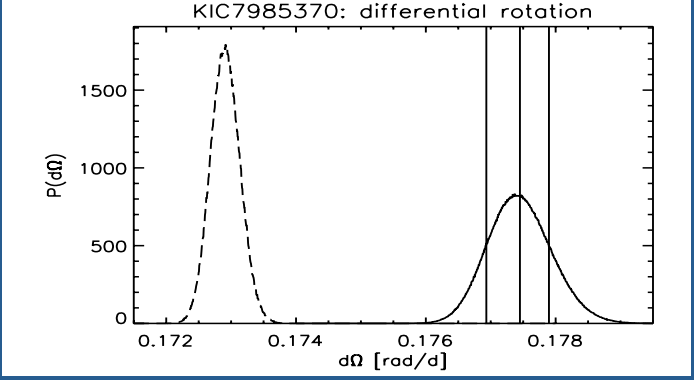

Limitations of few-spot models

- Significant light curve residuals with modulation in several cases (see below the cases of two stars modelled by Mosser et al. 2009);
- Large residuals during transits (or eclipses in the case of eclipsing close binaries);
- An unphysical averaging of the spot distribution over large areas, i.e., a few spots must account for the effect of many small active regions as in the Sun.

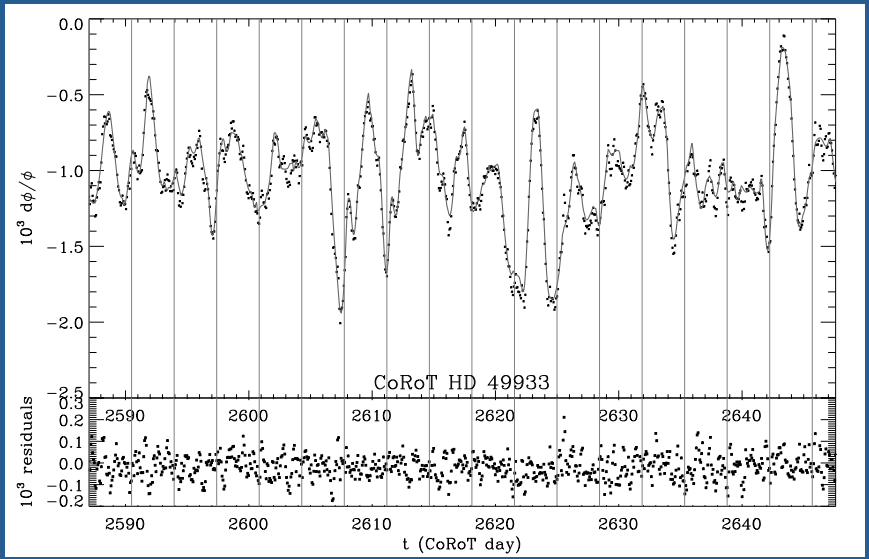

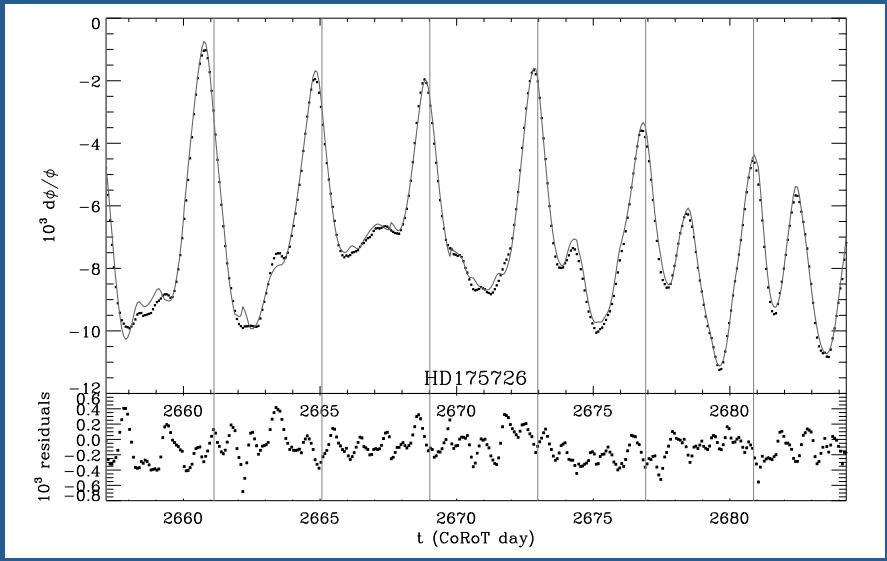

Continuous spot distributions

- Given the limitations of discrete spot models, an approach based on a continuous distribution of the spot filling factor has been proposed, similar to that adopted in the Doppler Imaging case;
- The intrinsic limitation of photometry is that it provides essentially 1D information while a map of the filling factor is a 2D object;
- The solution is generally non-unique and unstable, i.e., small variations in the data produce large changes in the map;
- A unique and stable solution can be obtained by including some a priori information on the map by means of a regularization approach (e.g., maximum entropy or Tikhonov regularizations).

Continuous distribution models

If the whole star is subdivided into N surface elements of area A_k, with $k = 1, 2, ..., N$, the flux coming from the k-th element is:

$$\delta F_k = I(\mu_k)(A_k \mu_k) v(\mu_k),$$

where

$$I(\mu_k) = f_{\rm s} I_{\rm s} + Q f_{\rm s} I_{\rm f} + [1 - (Q+1) f_{\rm s}] I_{\rm u}(\mu_k),$$

or, with a few algebra:

$$I(\mu_k) = \{1 + [c_{f0} Q(1 - \mu_k) - c_{\rm s}]\, f_{\rm s}\}\, I_{\rm u}(\mu_k)$$

The total flux coming from the disc is:

$$F(t) = \sum_{k=1}^{N} \delta F_k = \sum_k A_k I_{\rm u}(\mu_k)\, \{1 + [c_{f0} Q(1 - \mu_k) - c_{\rm s}]\, f_k\}\, v(\mu_k) \mu_k, \qquad (9)$$

where f_k is the spot filling factor (previously indicated with $f_{\rm s}$) and μ_k the projection factor of the k-th surface element at the time t.

In general, we want to compute M flux values $F_j \equiv F(t_j)$, where t_j, $j = 1, ..., M$ are the times of the observations. We shall denote them as the model vector $\mathbf{F}$. We can express its relationship to the distribution of the filling factor on the surface of the star by introducing a $M \times N$ projection matrix $\tilde{\mathbf{R}} = \{R_{jk}\}$ and a constant $F_{\rm u}$ that gives the unspotted flux as:

$$F_j \equiv F(t_j) = \sum_k R_{jk} f_k + F_{\rm u}, \qquad (10)$$

or, in matrix notation:

$$\mathbf{F} = \tilde{\mathbf{R}} \mathbf{f} + \mathbf{F}_{\rm u}, \qquad (11)$$

where $\mathbf{f} = \{f_k,\ k = 1, ...N\}$, is the vector of the filling factor on the surface of the star. If the observed flux values at the times t_j are denoted as the vector $\mathbf{D} = \{D_j,\ j = 1, ...M\}$, the χ^2 corresponding to a given distribution of the filling factor is:

$$\chi^2(\mathbf{f}) \equiv \sum_{j=1}^{M} \frac{(D_j - F_j)^2}{\sigma_j^2}, \qquad (12)$$

where σ_j is the standard deviation of the flux measurement D_j.

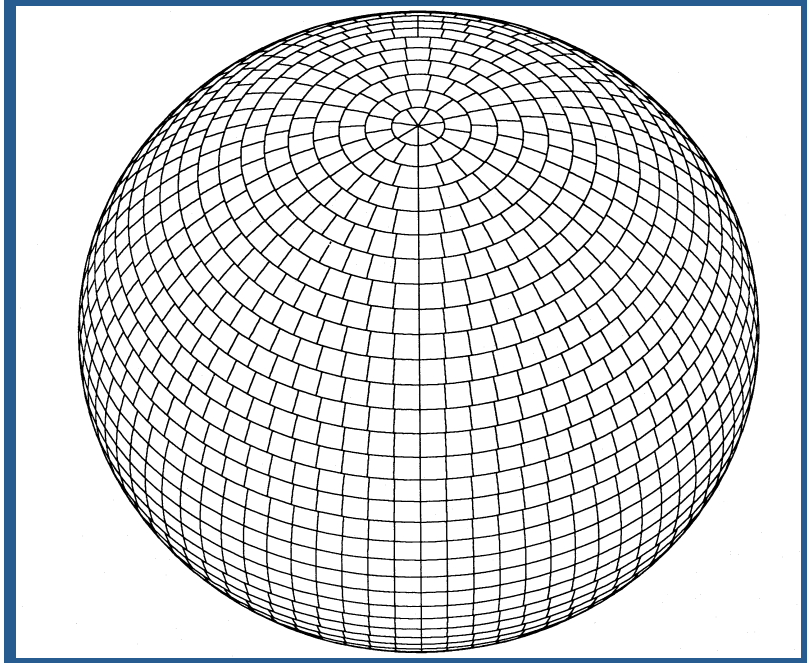

(picture from Vogt et al. 1987)

Regularized spot maps: ME

The regularized solution is computed by minimizing an objective function Z defined as a linear combination of the χ^2 and the regularizing functional S (for the Maximum Entropy case):

$$Z(\mathbf{f}) = \chi^2(\mathbf{f}) - \lambda_{\rm ME} S(\mathbf{f}), \tag{13}$$

where $\mathbf{f} = \{f_k,\ k = 1, ...N\}$ is the vector of the spot filling factors for the individual surface elements, $\lambda_{\rm ME}$ a Lagrangian multiplier, and

$$S = -\sum_k w_k \left[f_k \log \frac{f_k}{m} + (1 - f_k) \log \frac{(1 - f_k)}{(1 - m)} \right], \tag{14}$$

is the entropy functional, where w_k is the relative area of the k-th surface element and $m = 10^{-6}$ is a default minimum spot filling factor included to avoid the divergence of the logarithm.

S gets its maximum value for an immaculate star, i.e., $f_k = m$ in each surface elements.

The effect of the regularization is that of reducing the spot filling factor (or the spotted area) as much as possible, compatibly with fitting the data, by increasing the Lagrangian multiplier.

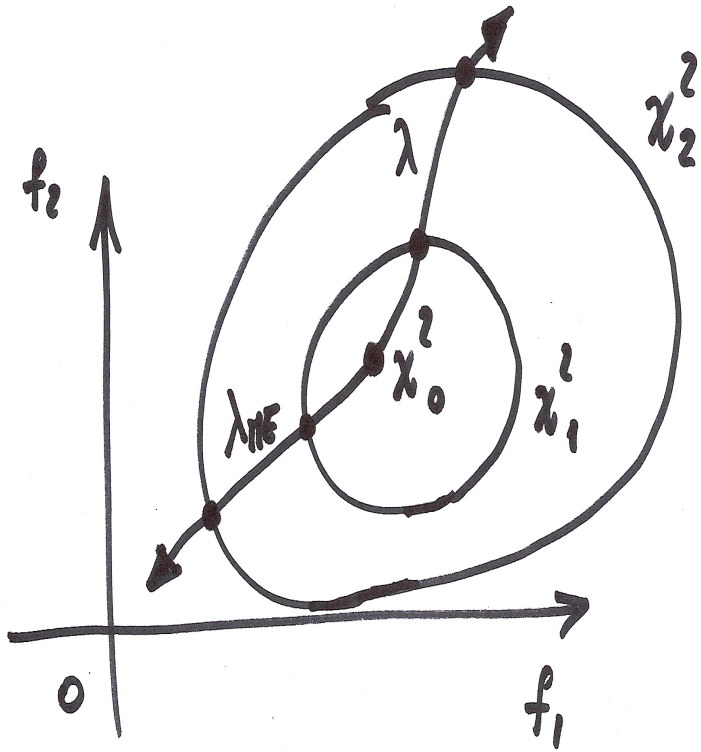

How to fix the regularization

- Without regularization ($\lambda_{\rm ME} = 0$), the best fit has the minimum $\chi^2 = \chi^2_0$ and the residuals of the fit have a Gaussian distribution with mean value $\mu = 0$ and a standard deviation σ. However, the fit is not acceptable because we also fit the noise;
- With the regularization, ($\lambda_{\rm ME} > 0$), the fit has $\chi^2 = \chi^2_1 > \chi^2_0$ and the residual distribution is now centred at a value $\mu > 0$ because the spotted area is reduced.

We can fix the optimal value of λ by comparing μ with σ. A practical recipe adopted in the case of space-borne photometry with high signal-to-noise ($S/N \geq 100$) is to increase λ until:

$$\mu = \frac{\sigma}{\sqrt{M}},$$

where M is the number of data points in the light curve. The value of S/N is the ratio of the flux modulation amplitude to the standard deviation of the individual flux measurements.

When $S/N \approx 10 - 30$, we adopt a stronger regularization, i.e.:

$$\mu = \beta \frac{\sigma}{\sqrt{M}},$$

where $\beta = 2 - 3$ is a numerical factor.

A visual inspection of the fit is generally needed to find the largest possible acceptable deviations, i.e., to fix the appropriate value of β.

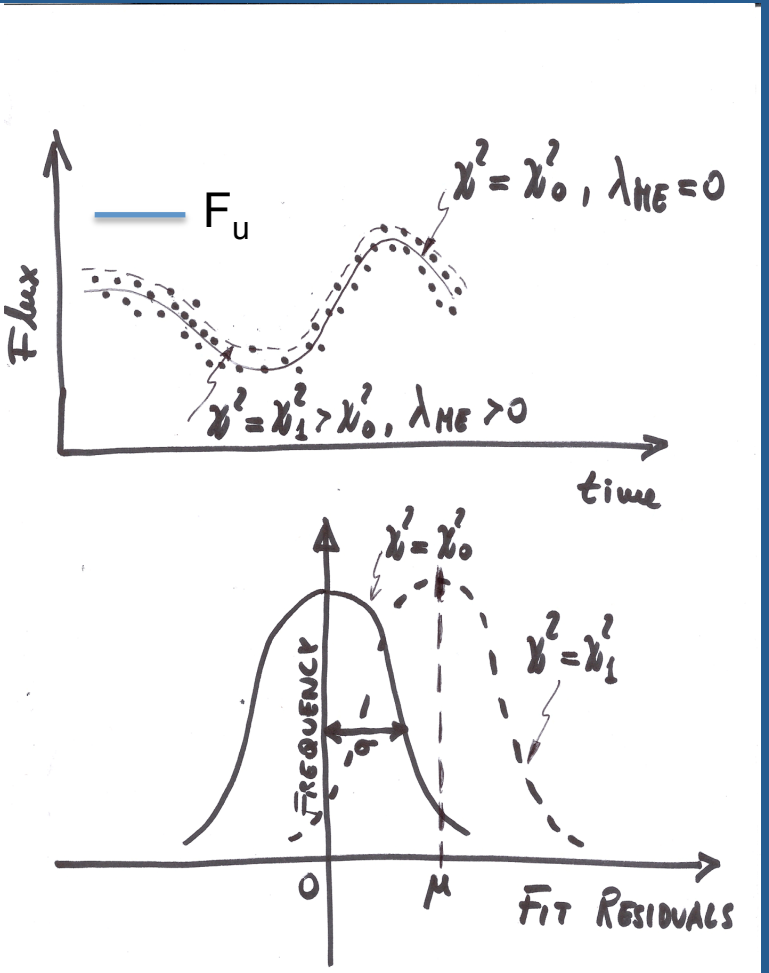

Other regularization approaches

- Several regularizing functionals can be used, e.g., the Tikhonov functional that makes the filling factor as smooth as possible (e.g., Piskunov et al. 1990);

$$T(\mathbf{f}) = \int_{\Sigma} \sum_{k=1}^{N} \left[\left(\frac{1}{R} \frac{\partial f_k}{\partial \theta} \right)^2 + \left(\frac{1}{R \sin\theta} \frac{\partial f_k}{\partial \phi} \right)^2 \right] d\Sigma,$$

where Σ is the stellar surface, R the radius of the star, θ the colatitude, and ϕ the longitude. The partial derivatives are numerically evaluated by the difference in the filling factors of neighbour surface elements.

- Other regularizing functionals have been proposed by, e.g., Harmon & Crews (2000) and applied to model Kepler light curves by, e.g., Roettenbacher et al. (2013).

Methods based on SVD

The χ^2 minimization problem to be solved to find $\mathbf{f}$ can be approached also by means of the Singular Value Decomposition (SVD) of the projection matrix $\tilde{\mathbf{R}}$. The method is described in, e.g., Press et al. 2007, *Numerical Recipes*, Ch. 15.4.2. Its advantages are:

- linear combination of the components of $\mathbf{f}$ that are not constrained by the data can be driven to zero (or to small, insignificant values);
- the solution is dominated by the linear combinations of the elements of $\mathbf{f}$ that produce most of the observed flux variations (the so-called principal components);
- the number of components to be retained in the solution is set by the minimum acceptable singular value;
- the error of the individual components can be evaluated starting from the error of the measurements.

Different versions of the approach have been implemented by, e.g., Berdyugina (1998, Occamian approach), or Savanov & Strassmeier (2005, 2008; Truncated LS Principal Components). They have also explored the performance of their approaches using synthetic datasets. Complex input spot distributions tend to be reconstructed as patches diffused all over the stellar surface.

Deriving robust results

- The dependence on the assumed stellar parameters, i, c_s, c_{f0}, and Q is still present in continuous filling factor maps;
- To reduce degeneracies, we focus on properties that are little affected by those parameters:
  - The relative distribution of the filling factor vs. longitude (collapse the 2D map into a 1D map by integrating over latitude); however, faculae may affect the distribution;
  - The *variation* of the total spotted area (because its absolute value depends on c_s, c_{f0}, Q, and F_u).

Testing ME spot modeling

- We used the time series of the Total Solar Irradiance with an accuracy of 20 ppm and 1 hr cadence to test different modelling approaches;
- The method based on a continuous distribution of spots and maximum entropy regularization proved to be the best one in comparison to 2-3 discrete spot models (see Lanza et al. 2007).

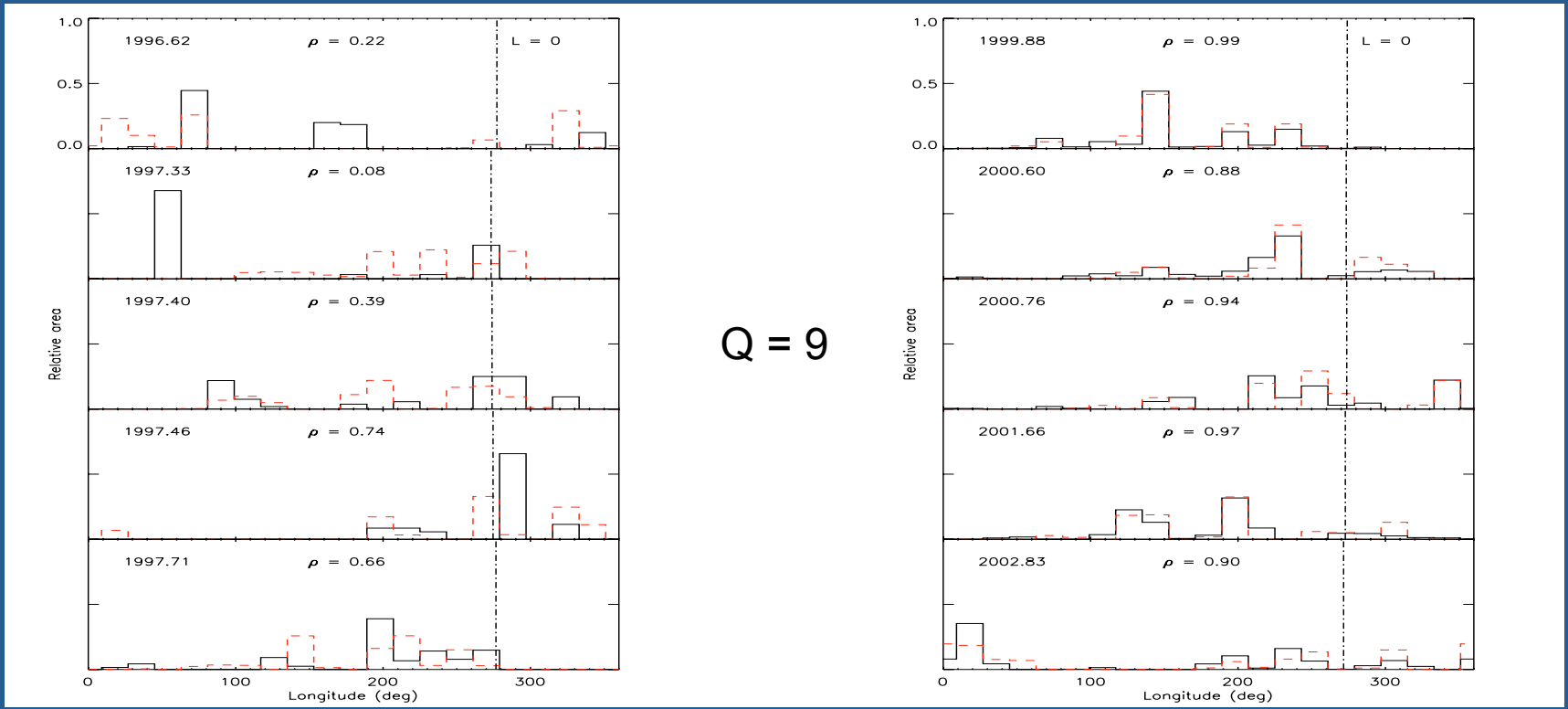

Starspot temperature from multiband photometry

- In principle, simultaneous multiband photometry can be used to measure starspot temperatures provided that the flux from the dark spots can be detected in some of the passbands;
- A good limb-darkening model is mandatory for accurate results;
- Spectrophotometry of TiO bands has also been applied because spots have T_{eff} similar to that of M-type stars in the case of G-K subgiants in RS CVn binary systems (e.g., O'Neal et al. 1996);
- Since most of the space-borne photometry is in a single passband (MOST, Kepler) or in passbands depending on the specific SED (CoRoT bright targets), here I shall focus on single-passband photometry.

Completely dark spot: effect of the limb darkening

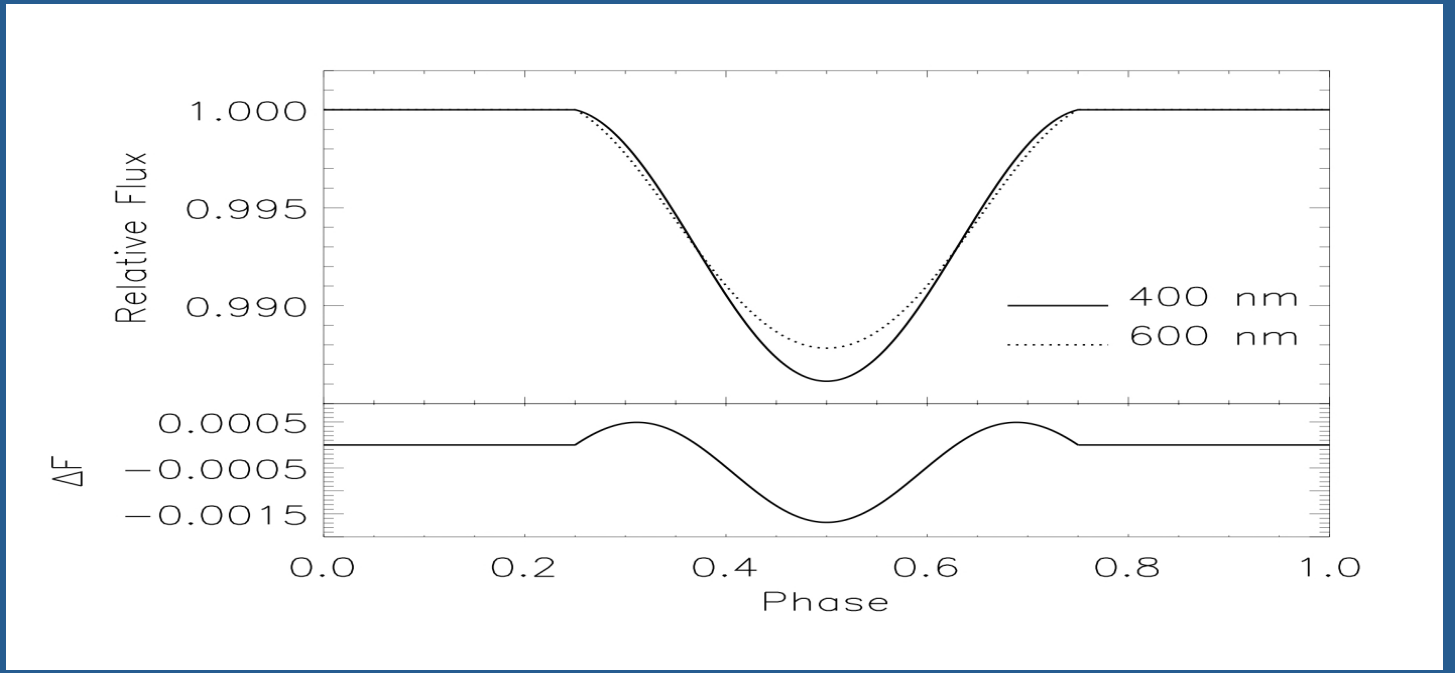

- The wavelength dependence of the limb-darkening introduces a color variation even in the case of a completely dark spot (T_{eff} = 0 K);
- Here I show the light variation in the case of a Sun-like star observed at 400 and 600 nm;
- Therefore, for an accurate estimate of starspot temperatures, we need an accurate limb-darkening model.

Spot mapping as a general inverse problem

Applying Fourier analysis

$$F(t) = \oint K(\mathbb{G}, \theta, \phi, t) M(\theta, \phi)\, \mathrm{d}\Omega,$$

where *K* is the projection kernel, *M* the surface map, $\mathbb{G}$ represents the geometry (inclination of the spin axis), θ is the colatitude, ϕ the longitude, *t* the time, Ω the solid angle.

$$M(\theta, \phi) = \sum_{l=0}^{\infty} \sum_{m=-l}^{l} C_l^m Y_l^m(\theta, \phi),$$

$$F_l^m(t) = \oint K(\theta, \phi, t) Y_l^m(\theta, \phi)\, \mathrm{d}\Omega.$$

$$C_l^m = \frac{1}{4\pi} \oint M(\theta, \phi) Y_l^m(\theta, \phi)\, \mathrm{d}\Omega.$$

$$F^m(t) = \sum_{l=|m|}^{\infty} C_l^m F_l^m(t),$$

There is an infinite number of harmonics contributing to the component of the light curve with a given *m*.

An ill-posed problem

- Even in the case of a noiseless light curve, the solution is non-unique;
- There are non-zero maps that produce flat light curves (the so-called *nullspace*);
- Cowan et al. (2013) have characterized the nullspace (see also Russell 1906); for example in the case of a star viewed equator-on:

$$F_l^m(t) = \begin{cases} 1 & \text{if } l = 0 \\ \frac{2}{\sqrt{3}} \cos\phi_0 & \text{if } l = 1 \text{ and } m = 1 \\ \frac{2(-1)^{m/2}}{\pi(1-m^2)} \sqrt{\frac{2(l-m)!}{(2l+1)(l+m)!}} \left[R_{l+1}^{m+1}(\text{odd}) - R_{l-1}^{m+1}(\text{odd}) \right] \cos(m\phi_0) & \text{if } l \text{ and } m \text{ are even} \\ 0 & \text{otherwise,} \end{cases}$$

ϕ_0 is the longitude of the observer (fixed in the adopted frame) and R_l^m (odd) are numerical coefficients (see Cowan et al.); for simplicity, limb-darkening is not considered.

Note that the amplitude of the Fourier components decreases rapidly with increasing azimuthal order *m.*

An example of a nullspace map

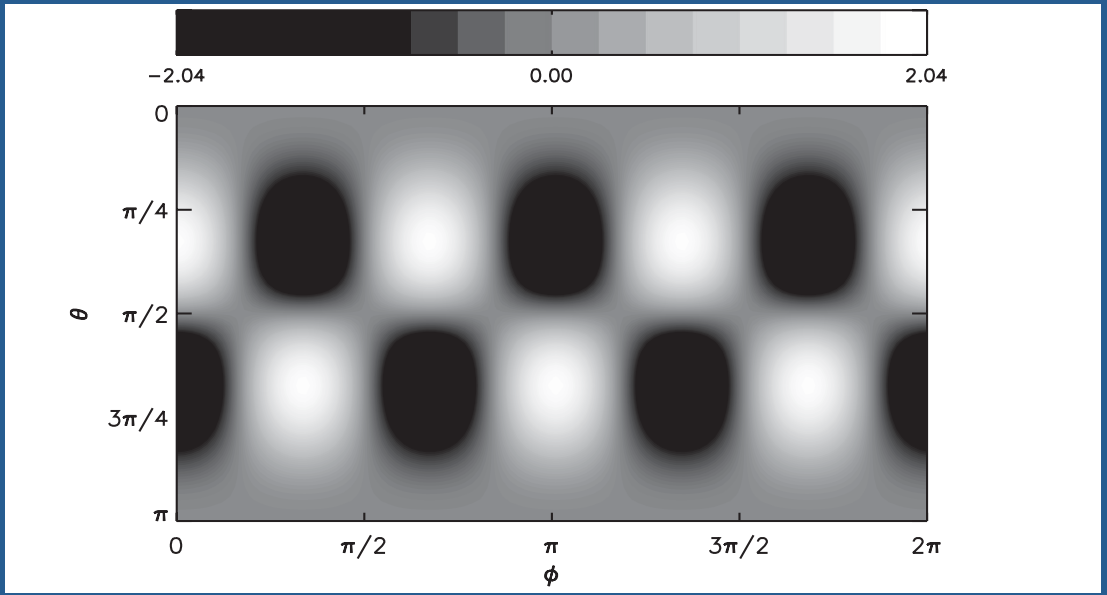

The Y_4^3 map in the nullspace of the light curve for a star without limb darkening viewed equator-on.

(see Cowan et al. 2013)

Properties of the light variations due to spots

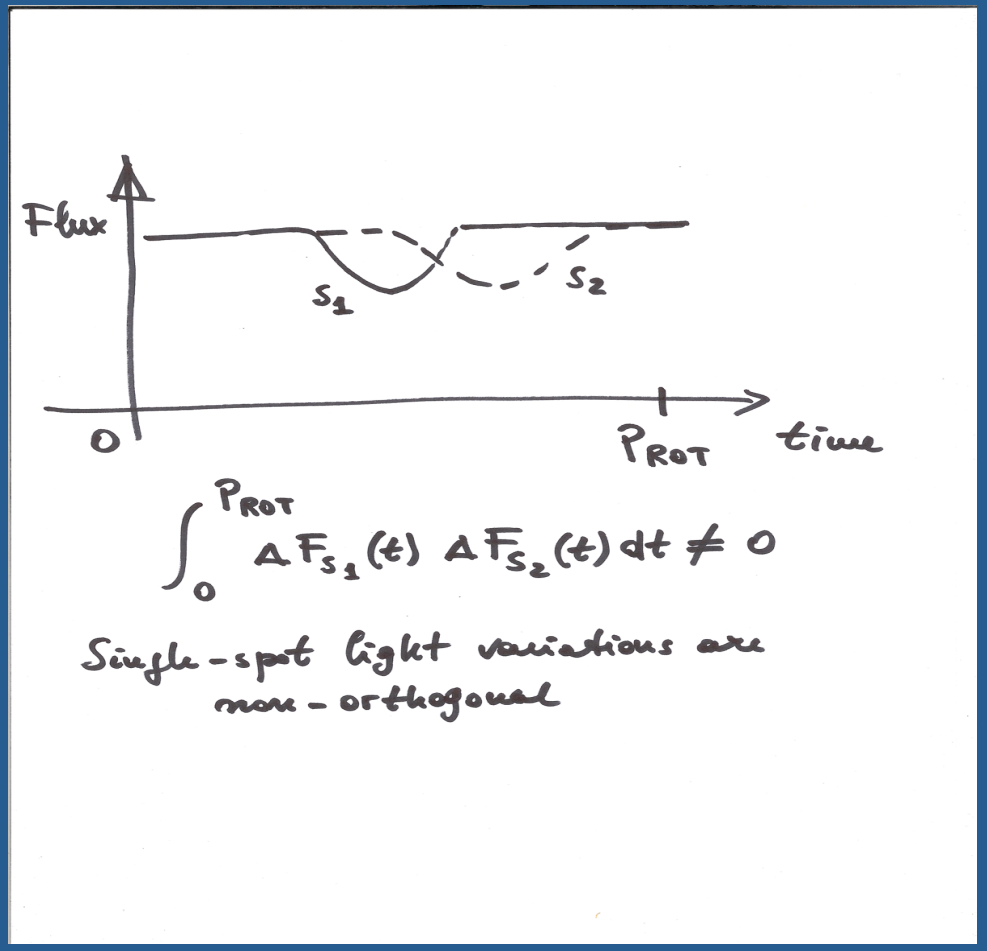

Planetary transits

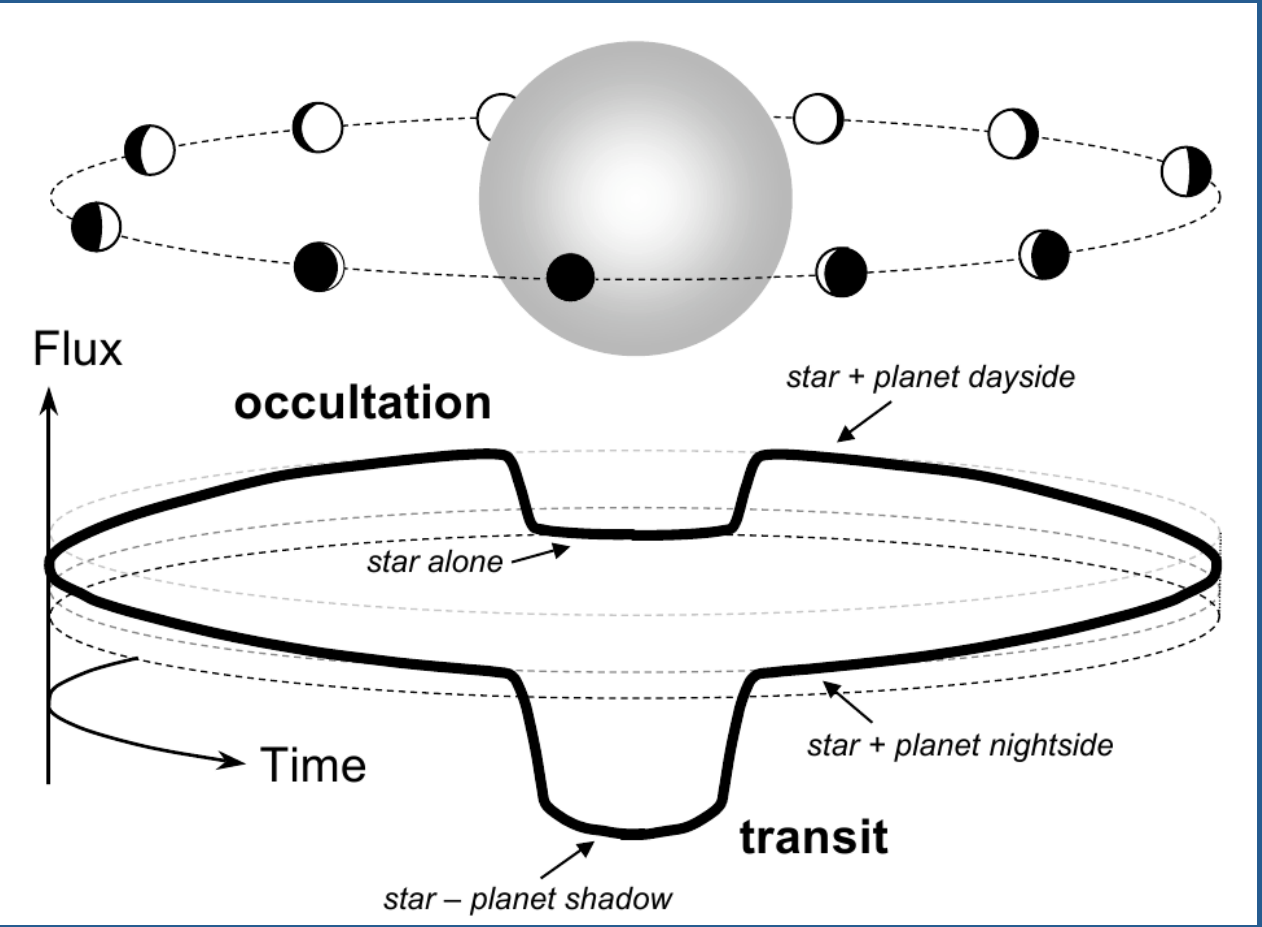

Planetary transits

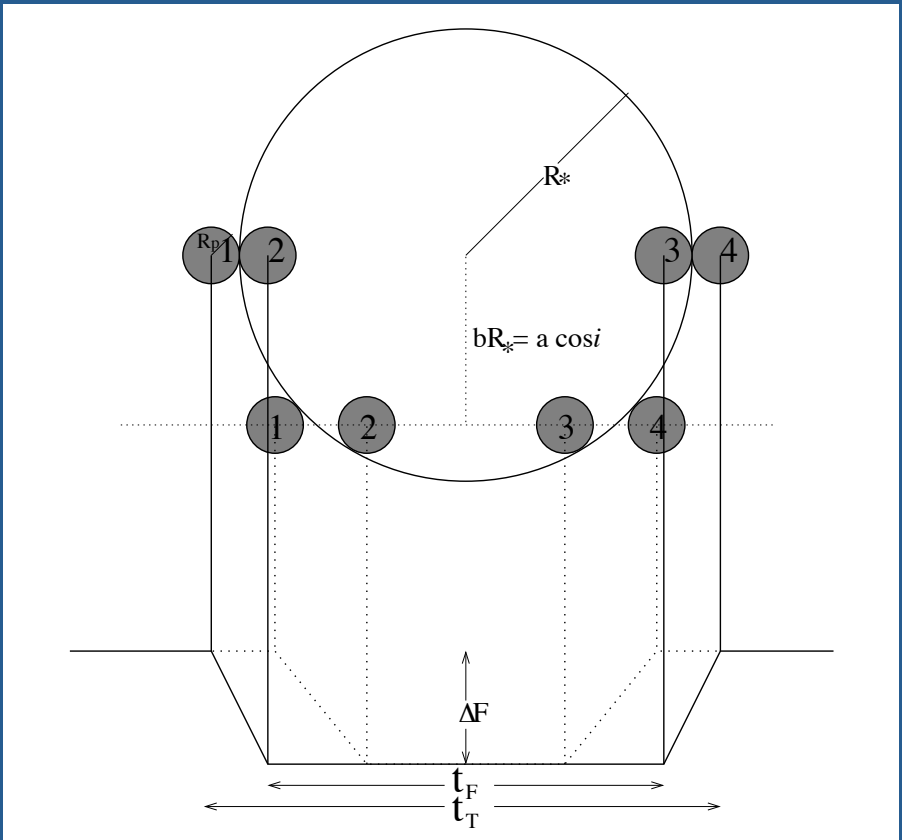

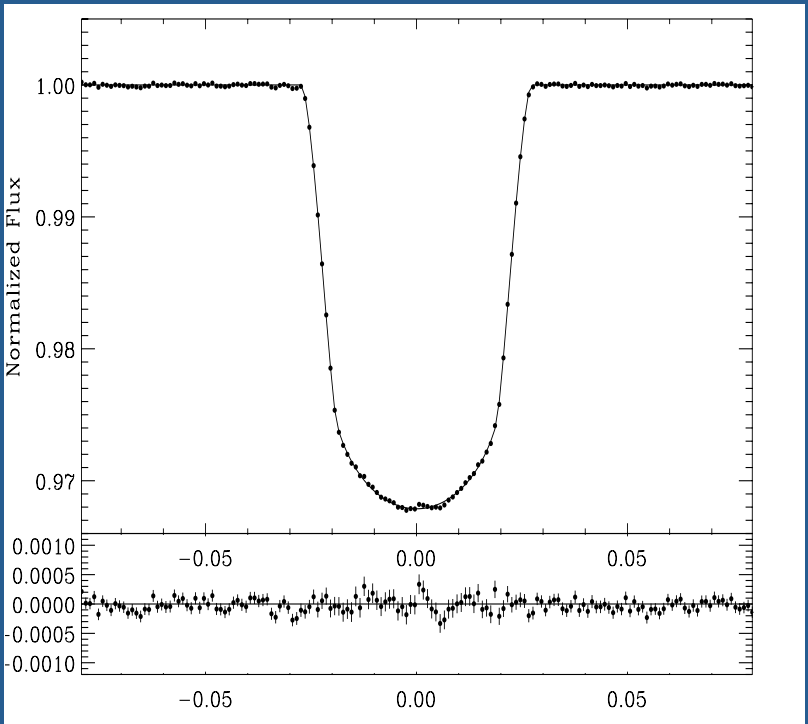

Left: Light curve of planetary transit on an ideal star without limb darkening (Seager & Mallen-Ornelas 2003). *Right:* transit of the planet of CoRoT-2 (a real, limb-darkened star; Alonso et al. 2008).

Rossiter-McLaughlin effect

- The Rossiter-McLaughlin (RM) effect is an anomaly of the stellar radial velocity detected during transits;
- The angle between the projections on the plane of the sky of the spin axis and the normal to the orbital plane can be measured by exploiting the RM effect;
- This provides complementary information on the inclination of the stellar spin axis to the line of sight in the case of transiting systems.

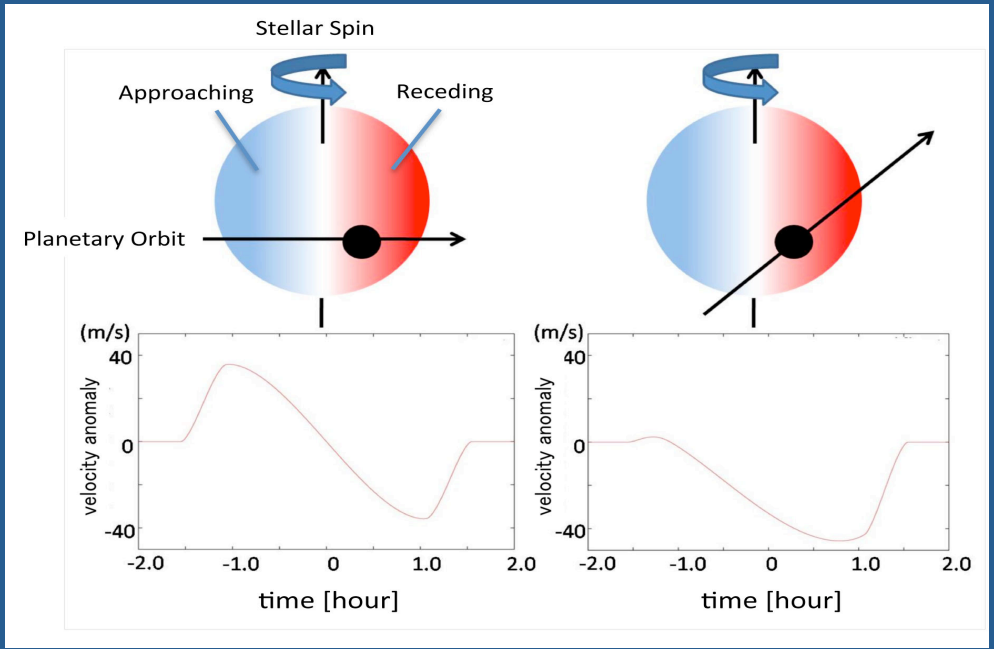

Some selected results

CoRoT-2

- A main-sequence G7 star (V=12.6), accompanied by a hot Jupiter with an orbital period of 1.743 d (Alonso et al. 2008; Bouchy et al. 2008);

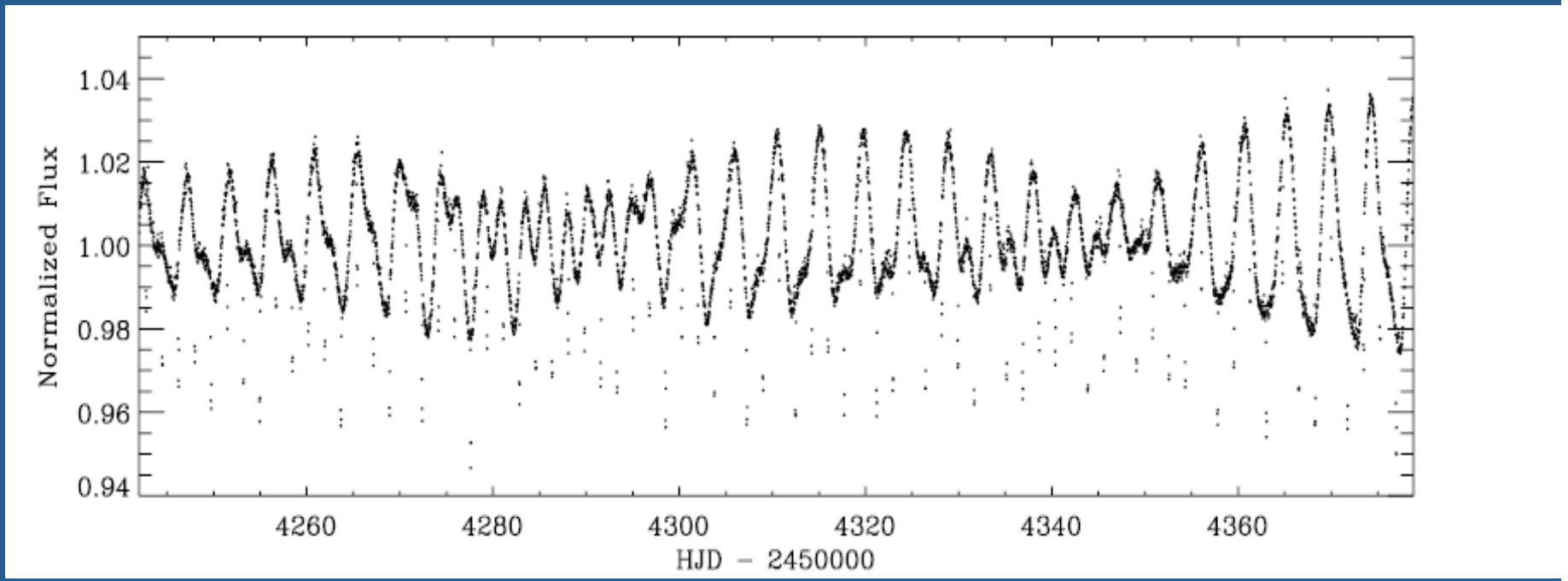

ME best fit of the out-of-transit light curve

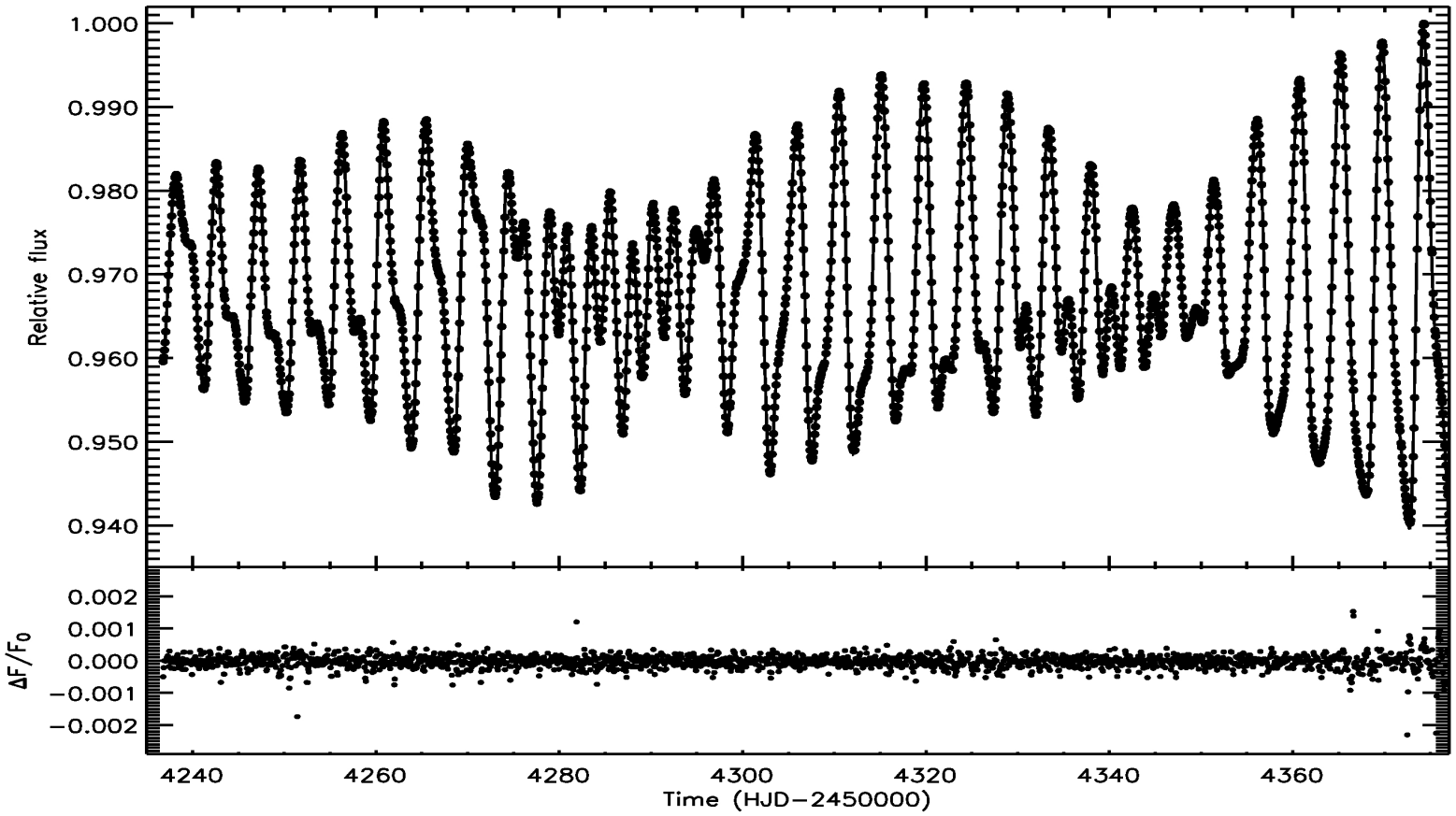

(normal points obtained by binning the data along each satellite orbital period of 6184 s)

Spot area vs. longitude and time

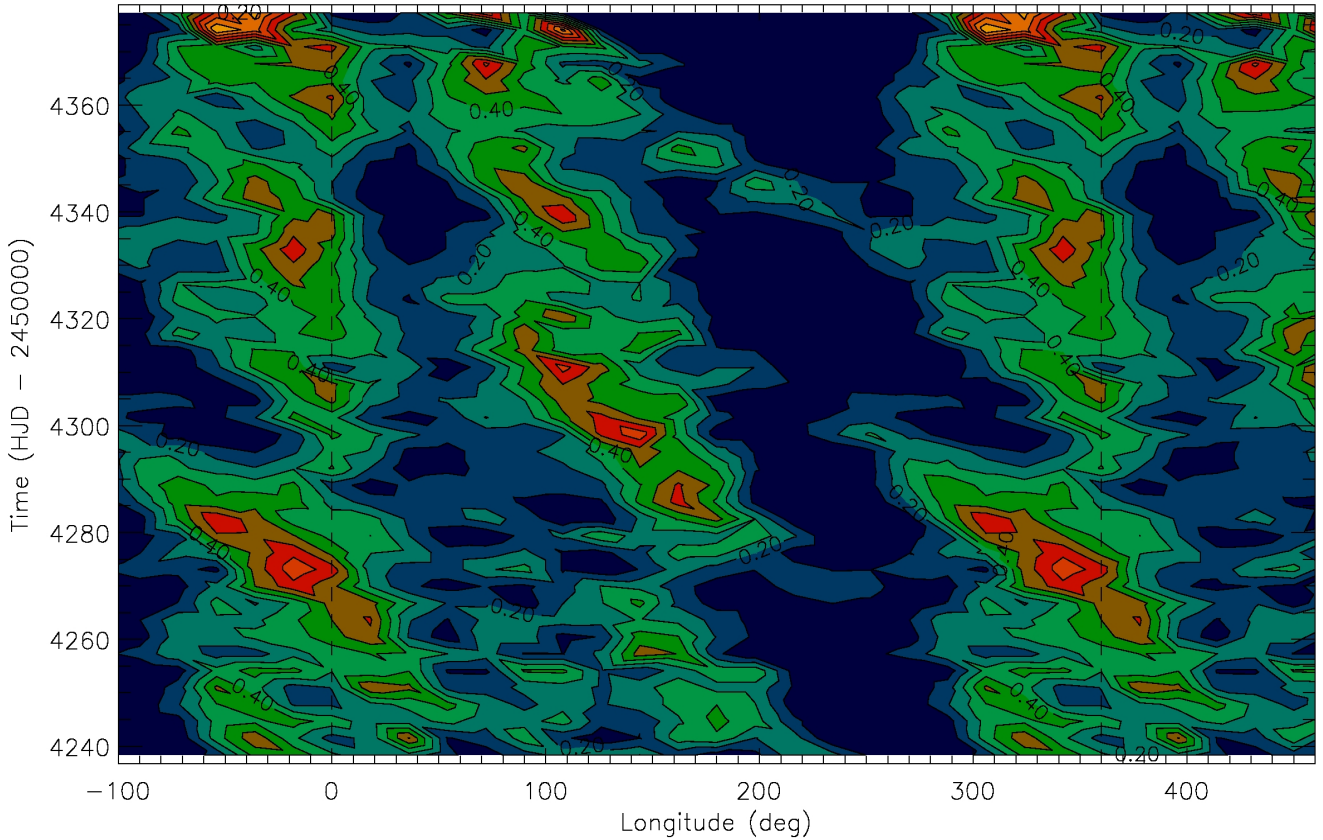

(The rotation period of the longitude reference frame is 4.5221 days)

Differential rotation in CoRoT-2

- Individual spot groups migrate backward in longitude during their lifetime, i.e., their angular velocity is lower than that of the active longitudes (cf. *sunspot group braking*; Zappalà & Zuccarello 1991; Schuessler & Rempel 2005);

- One of the *active longitudes* is almost fixed while the other migrates backward, suggesting a surface differential rotation with a relative amplitude $\Delta\Omega/\Omega \approx 0.9$ percent (this is actually *a lower limit* to $\Delta\Omega/\Omega$);

- Modelling the migration of *individual spots,* a higher differential rotation is derived: $\Delta\Omega/\Omega \approx 8$ percent (Fröhlich et al. 2009; Huber et al. 2010).

Variation of the spot area vs. time (a possible Rieger cycle)

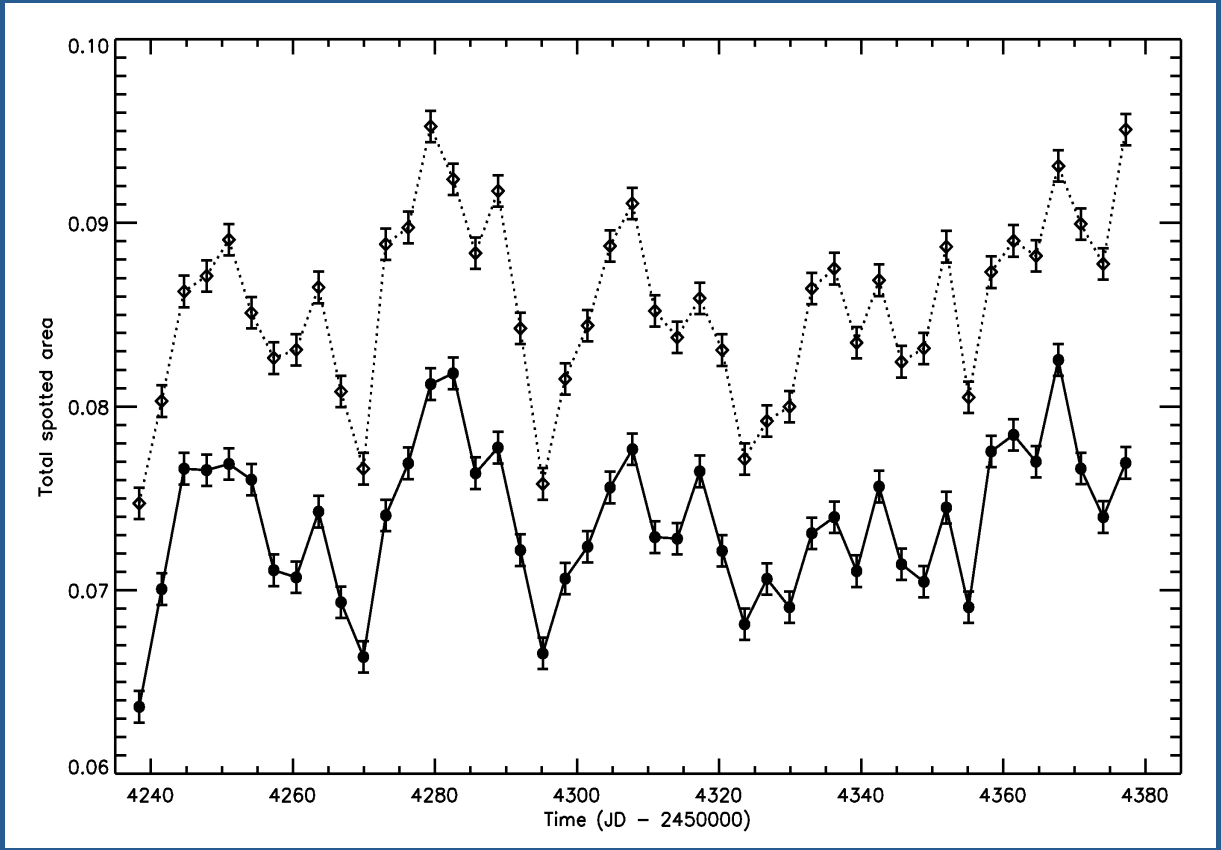

Spots only (solid line): P_{cyc} = 28.9 ± 4.8 d;
Spots and faculae with $Q \equiv A_f/A_s$ = 1.5 (dot-dashed line): P_{cyc} = 29.5 ± 4.8 d;

Solar Rieger cycles

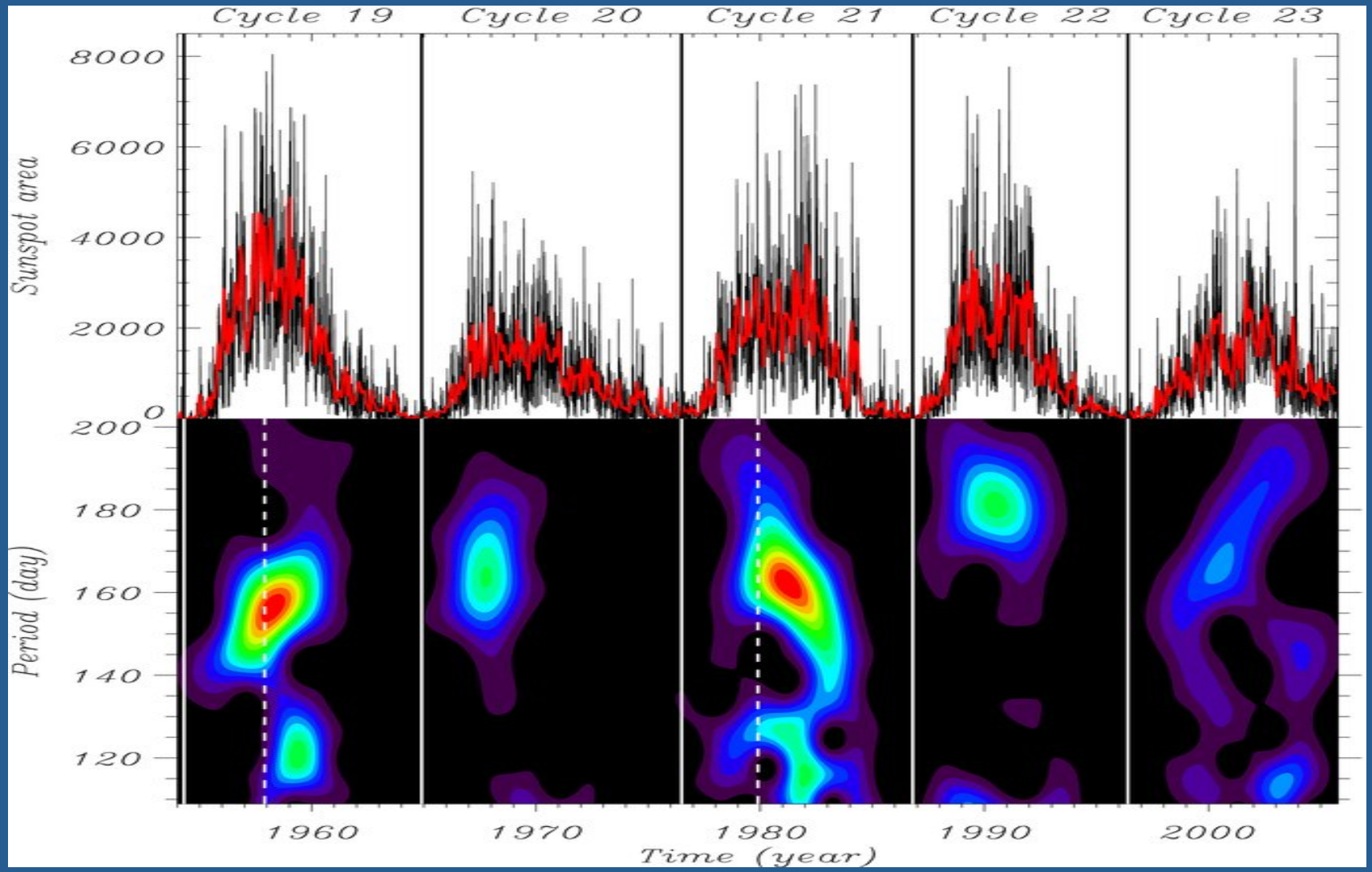

Wavelet analysis of sunspot area variation (after Zaqarashvili et al. 2010; see the original discovery paper by Oliver, Ballester & Baudin 1998, in Nature).

Possible origin of the Rieger cycle in CoRoT-Exo-2a

a) Rossby-type waves trapped in the outer layers of the stellar convection zone, as suggested for the Sun (Lou 2000):

$$\omega_{Rossby} \propto \Omega;$$

b) a possible star-planet magnetic interaction: the synodic period of the planet with respect to the stellar rotation period is 2.89 days (i.e., $1/P_{syn} = 1/P_{orb} - 1/P_{rot}$);

(see Lanza et al. 2009a for details).

Comparison with Huber et al.

- Huber et al. (2010) published another model of CoRoT-2 light curve, but with an approach different from that of Lanza et al. (2009a);
- They subdivided the star into longitudinal sectors and varied their brightness to fit the light curve;
- Different longitudinal extensions for occulted and unocculted sectors are used;
- They obtained a good best fit with 12 non-occulted sectors and 24 occulted sectors.

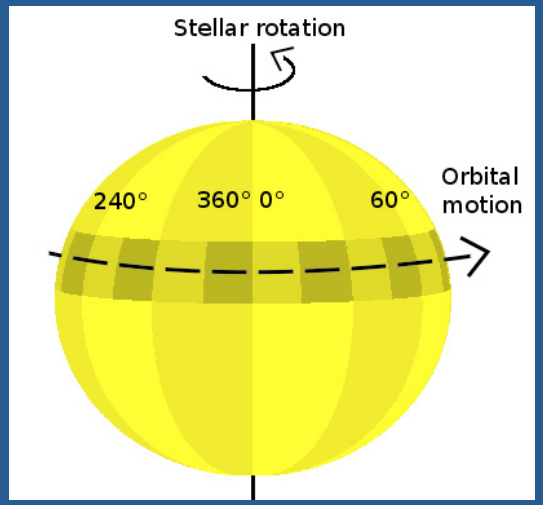

(Huber et al. 2009)

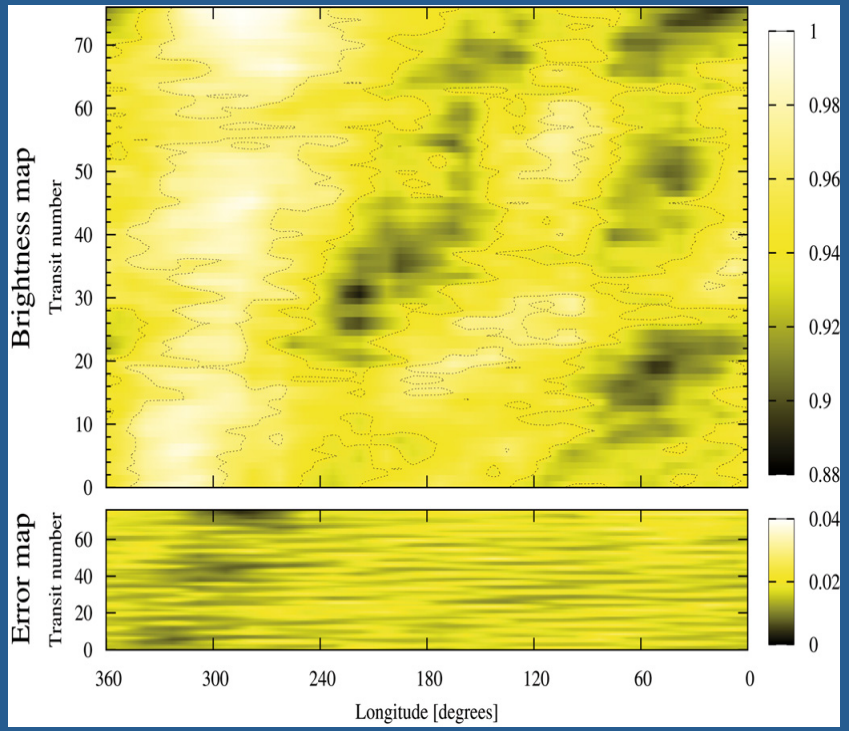

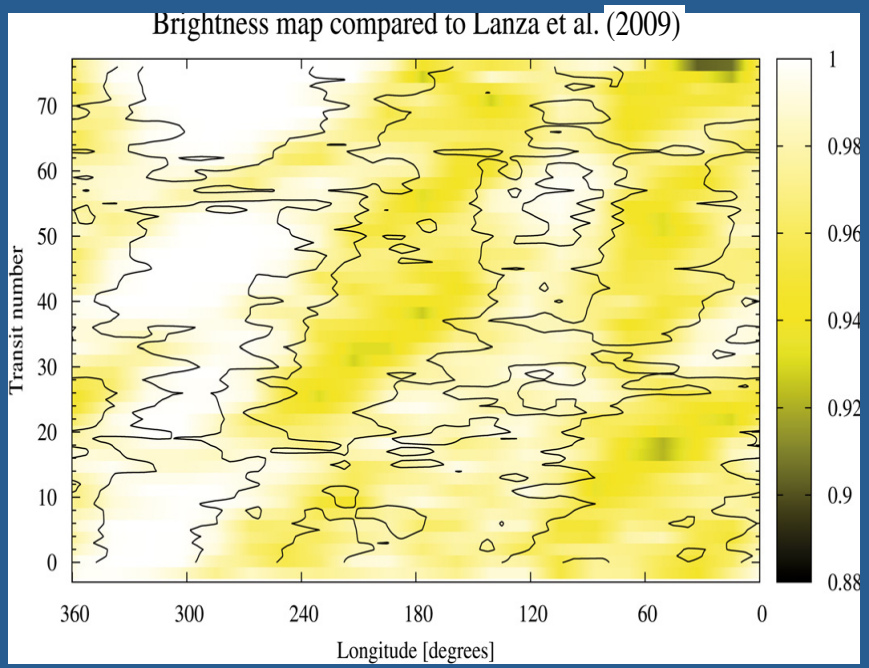

Left: Spot map of CoRoT-2 obtained by Huber et al. (2010) by fitting the entire light curve (in and outside transits). Right: comparison of their map (contours) with that of Lanza et al. (2009a) (color shades); the latter is based only on the out-of-transit light curve.

Model by Fröhlich et al. (2009)

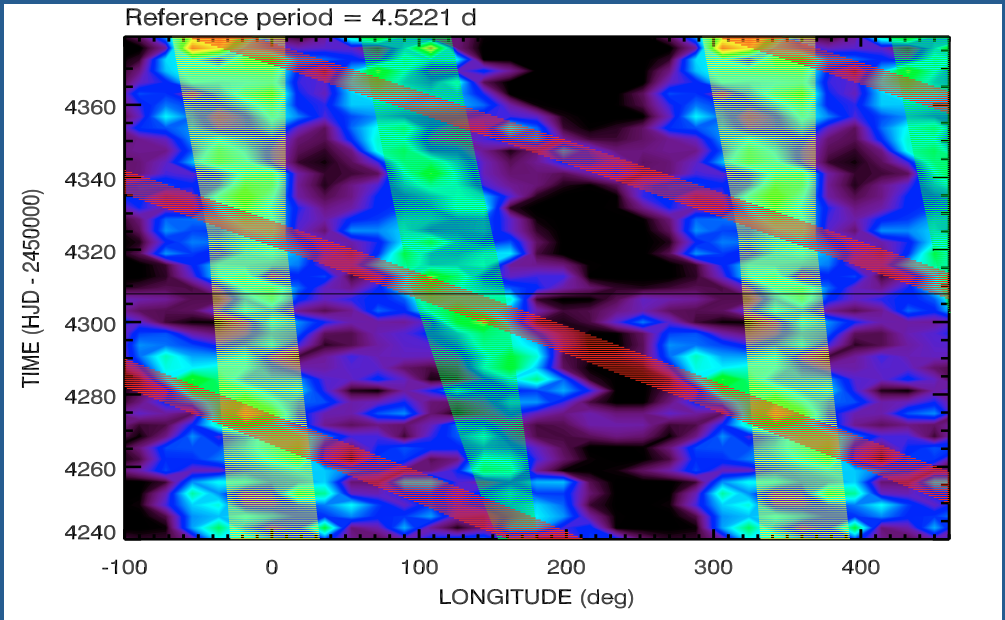

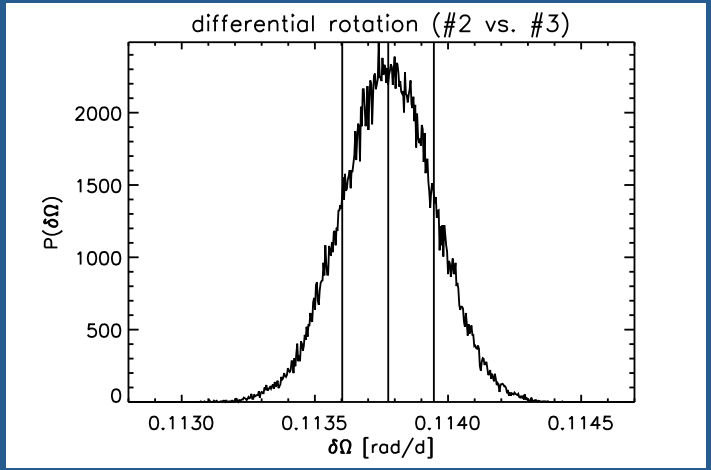

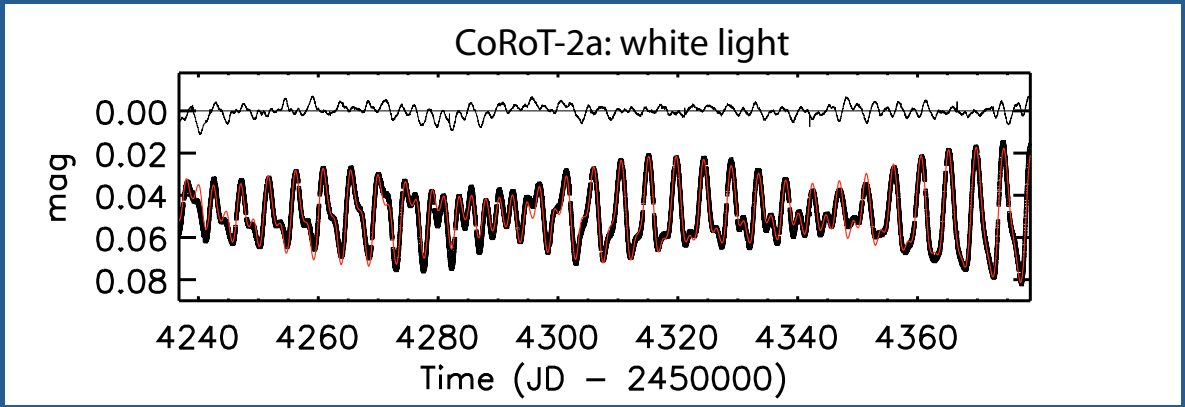

A Bayesian 3-spot model of CoRoT-2 light curve.

Out-of-transit light curve of CoRoT-4

CoRoT-4 is a F7 main-sequence star (V~13.7) accompanied by a transiting hot Jupiter with a period of 9.202 days (Aigrain et al. 2008; Moutou et al. 2008). The stellar rotation is quasi-synchronized with the orbit of the planet.

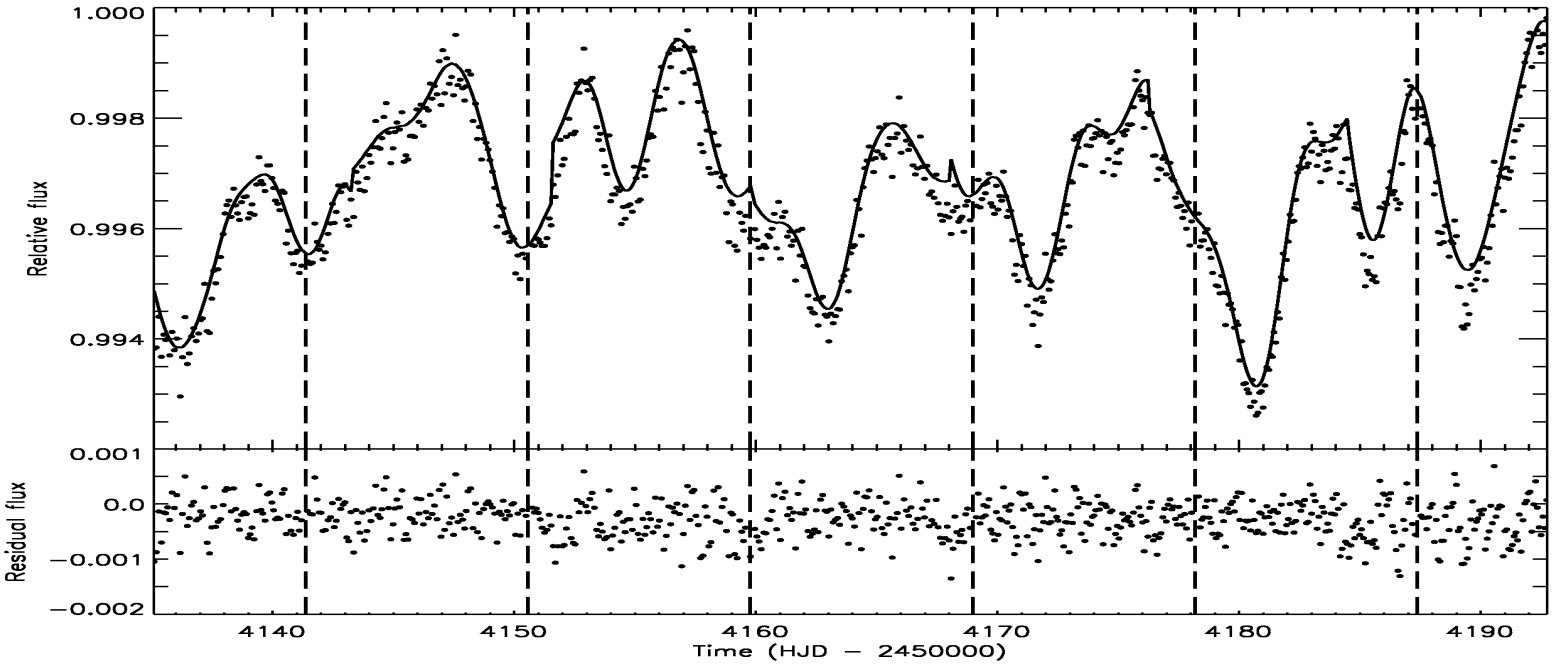

(normal points obtained by binning the observation along each CoRoT orbital period; solid line: ME best fit; dashed vertical lines mark the epochs of mid-transits).

Plots of the spotted area vs. longitude: Differential Rotation in CoRoT-4

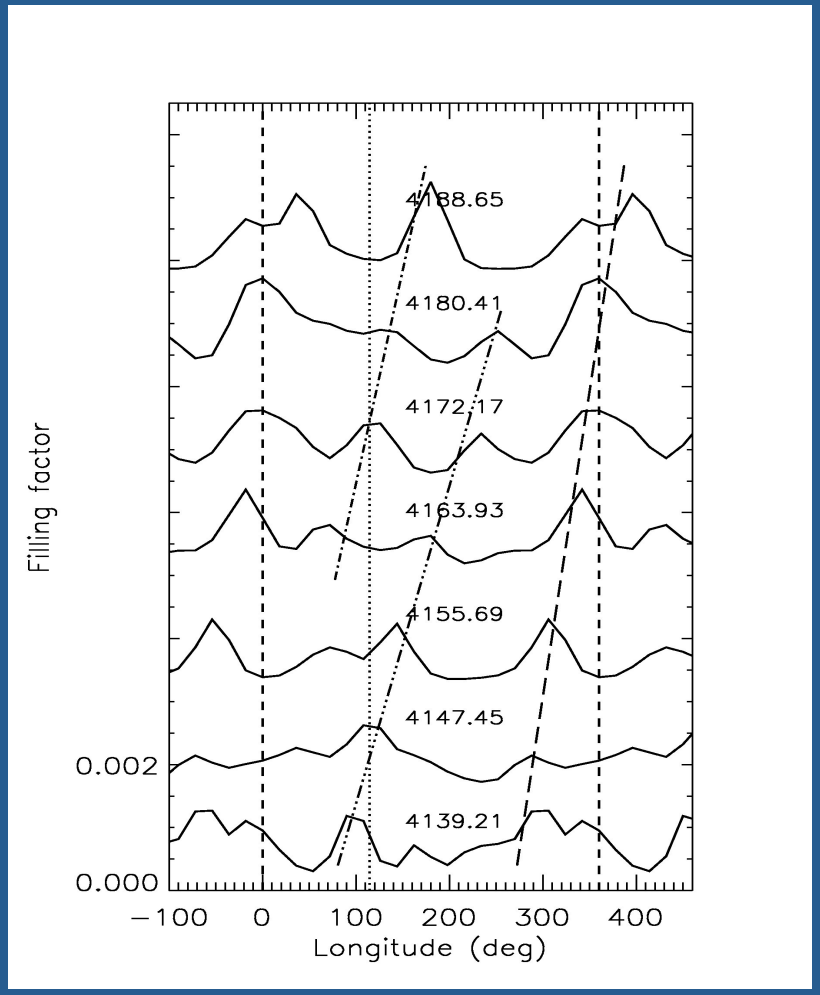

(Time labels are HJD-2450000.0)

Active longitude relative migration rates in a reference frame with a rotation period of 9.202 days:

a) long-dashed: $\Delta\Omega/\Omega = 0.052 \pm 0.010$;
b) 3-dot-dashed: $\Delta\Omega/\Omega = 0.108 \pm 0.010$;
c) dot-dashed: $\Delta\Omega/\Omega = 0.100 \pm 0.024$.

From the difference between the greatest and the lowest migration rates, we estimate:

$$\Delta\Omega/\Omega = 0.056 \pm 0.015$$

(Lanza et al. 2009b)

Differential rotation in CoRoT-7

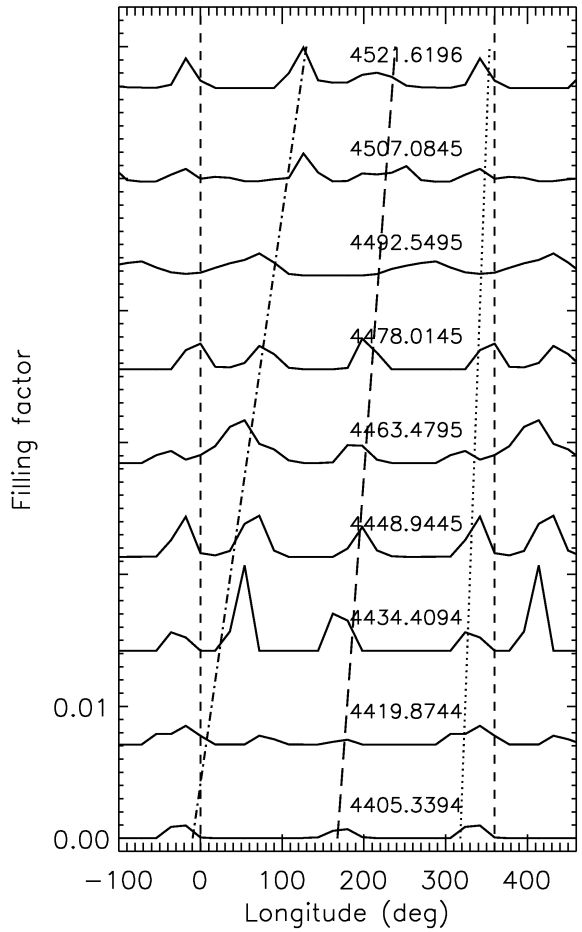

From the slowest and the fastest migrating active longitudes, we find:

$$\Delta\Omega/\Omega = 0.058 \pm 0.017$$

(Lanza et al. 2010)

Differential rotation in CoRoT-6

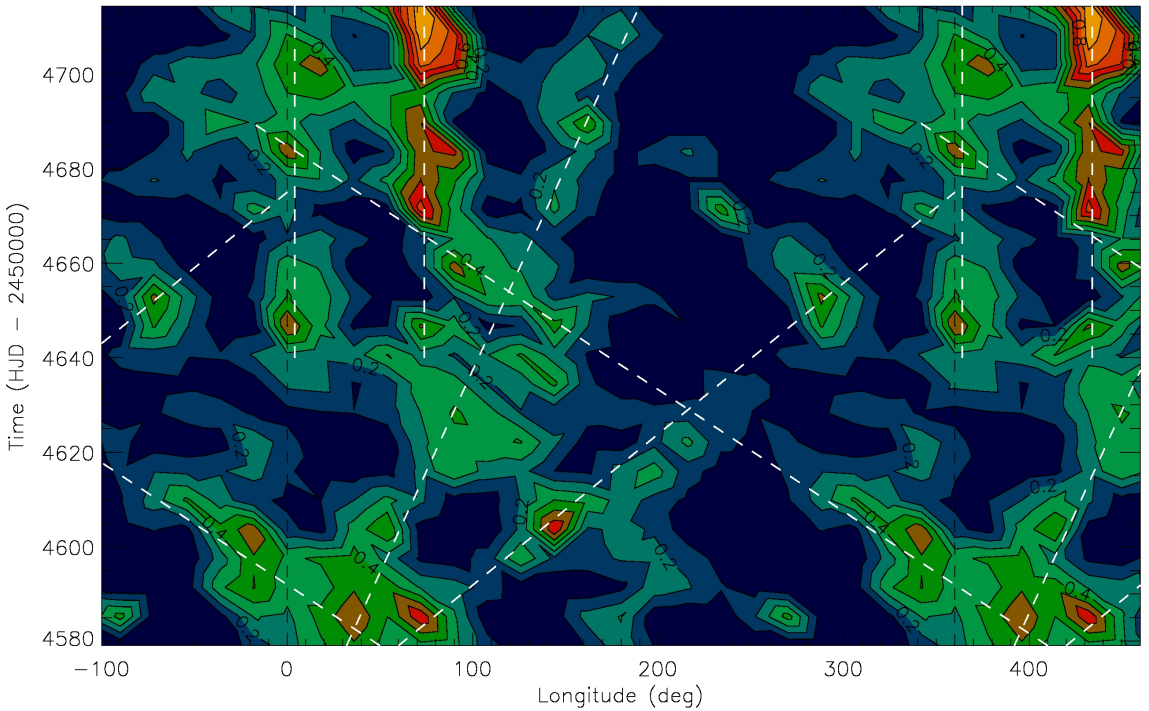

From the lowest and the fastest migrating active longitudes, we find $\Delta\Omega/\Omega = 0.12 \pm 0.02$ (Lanza et al. 2011a).

Differential rotation in late-type stars

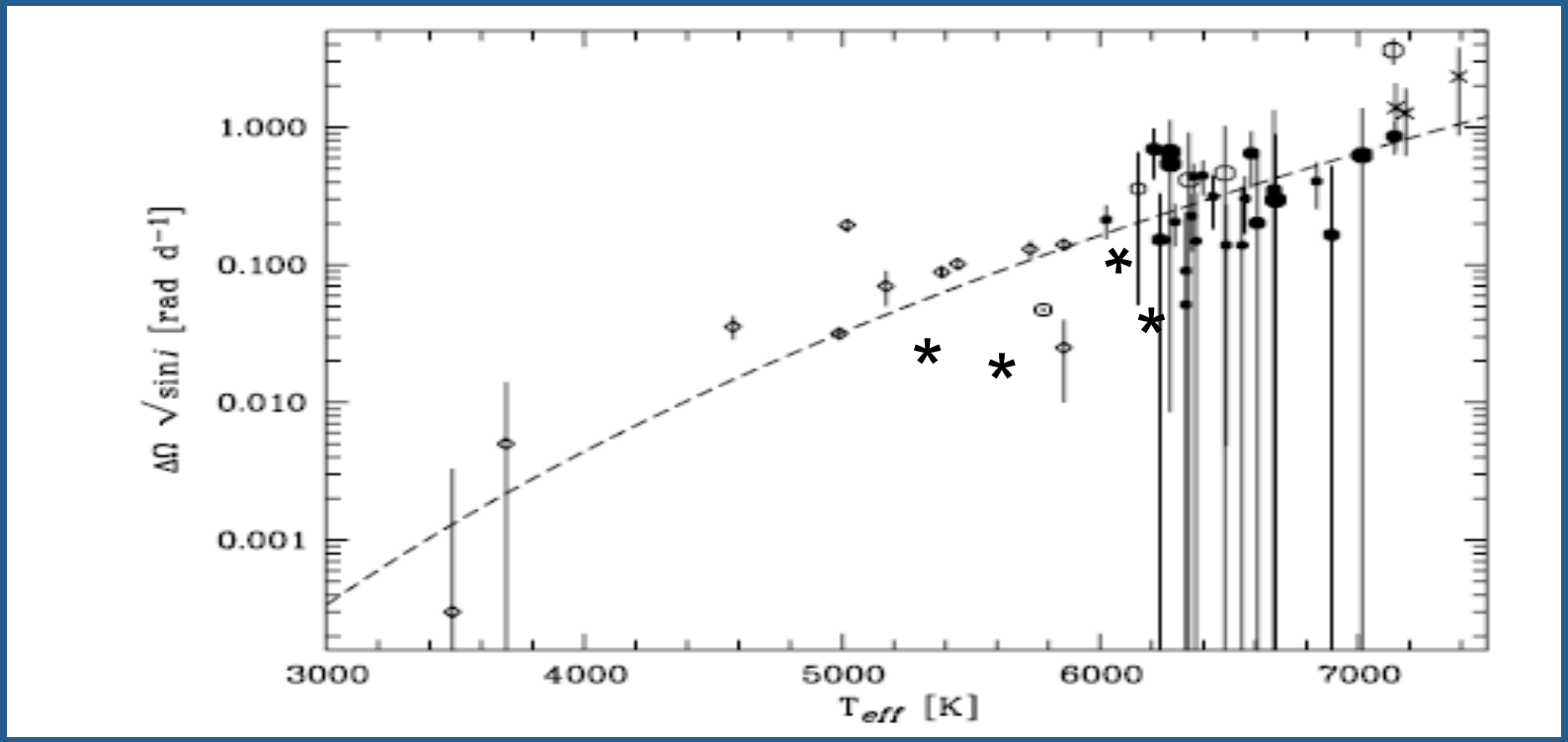

The asterisks indicate the values obtained for CoRoT-2, 4, 6, and 7; data for other stars are from Barnes et al. (2005) and Reiners (2006; Fig.5). The dashed line is the relationship derived by Barnes et al. (2005).

Kepler-17

- Bonomo & Lanza (2012) fitted the out-of-transit light curve of Kepler-17;
- They found active longitudes and a general correspondence with the spots occulted by the planet during transits;
- A Rieger-like cycle with a period of ≈ 48 days was detected in the second half of the dataset.

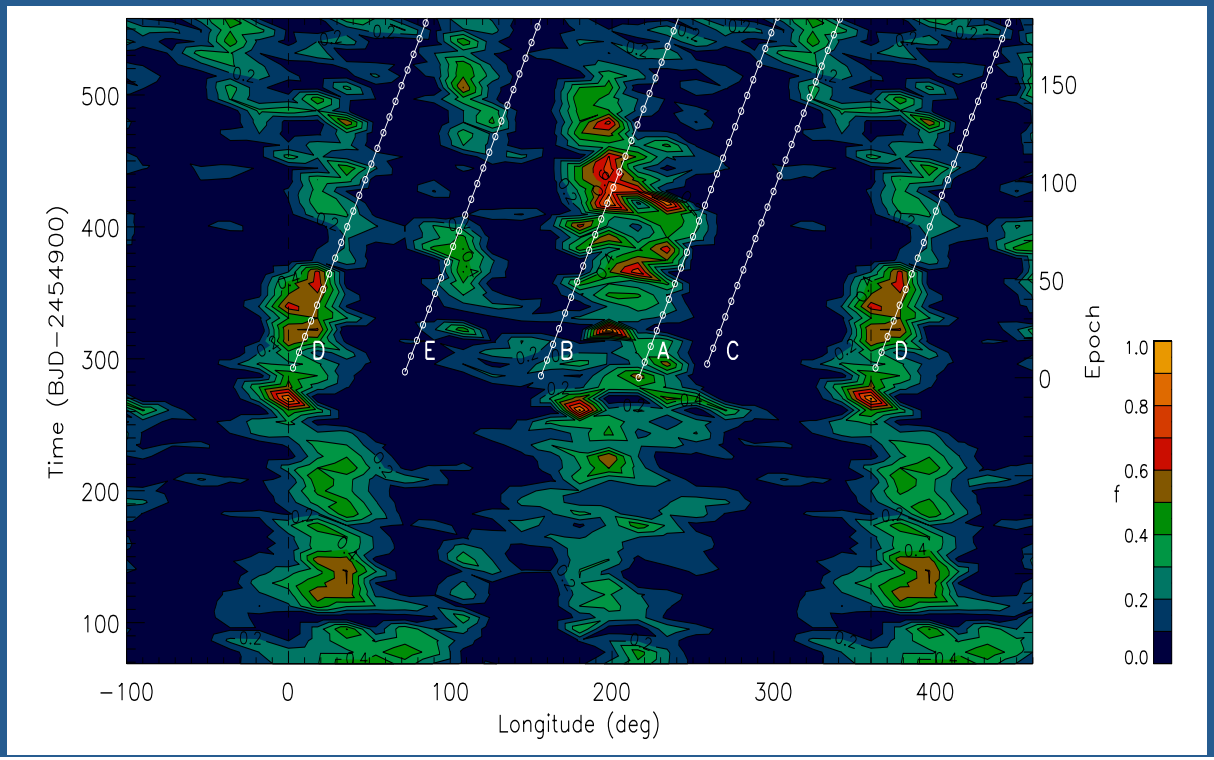

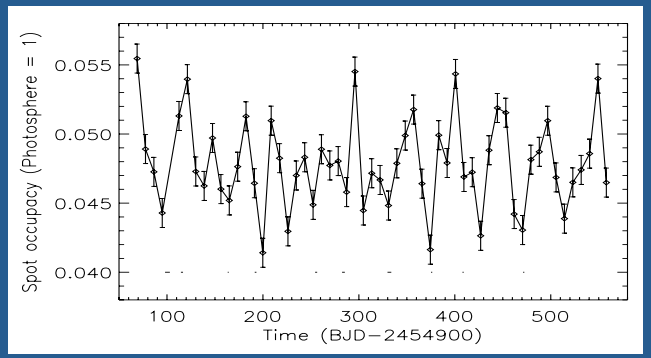

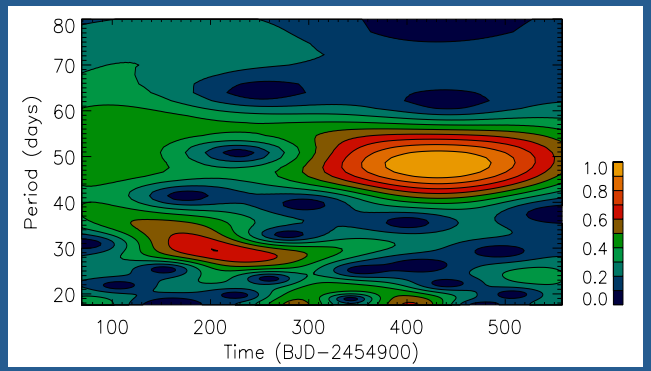

Possible star-planet interactions (SPIs)

- The planets of CoRoT-2, CoRoT-4, CoRoT-6, and Kepler-17 are *hot Jupiters*, i.e., giant planets orbiting within 0.15 AU from their host stars;

- They can interact through tides and magnetic fields with their host stars, possibly affecting their activity (e.g., Cuntz et al. 2000; Lanza 2008, 2009, 2011);

- Current evidence of magnetic SPI is limited to a few systems and at some epochs (e.g., Shkolnik et al. 2008; 2009).

Mean spotted area vs. longitude in CoRoT-4

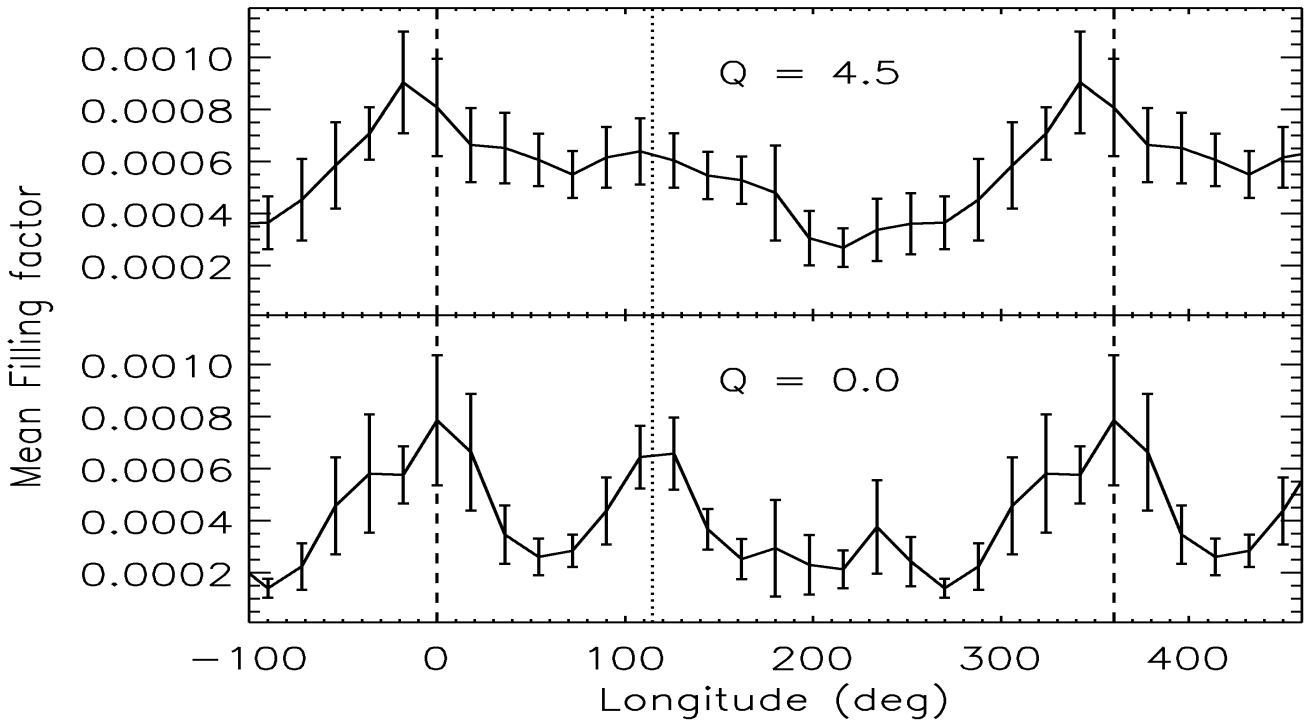

Time average of the spotted area vs. longitude; Q is the facular-to-spotted area ratio adopted in the models, thus models with Q=0 do not include faculae. The dotted line marks the subplanetary longitude.

Possible star-planet interaction in CoRoT-6

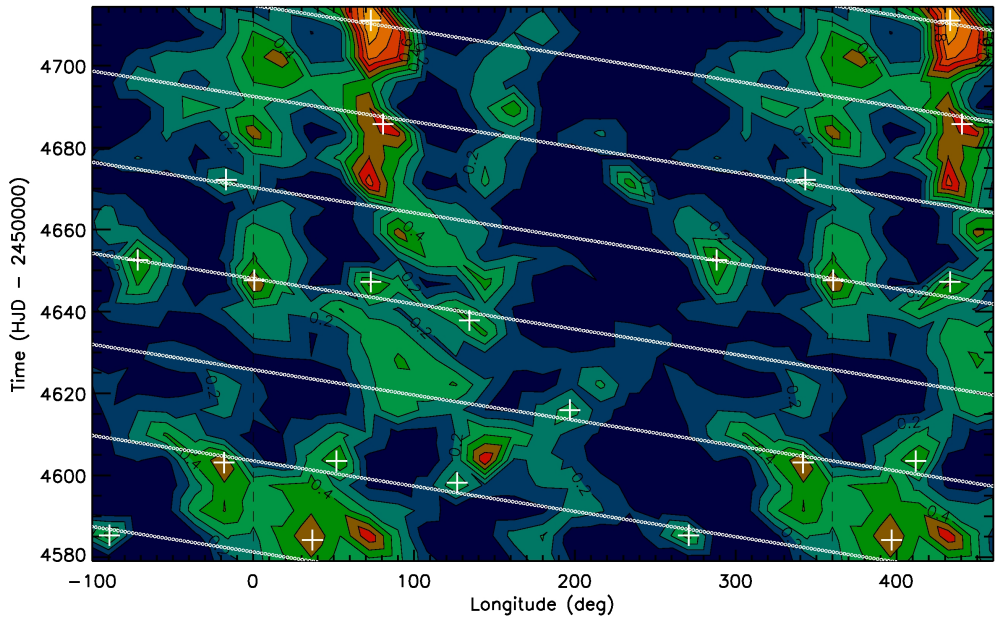

The straight lines mark a longitude at -200° from the subplanetary longitude; the crosses mark the active regions possibly associated with that point. The probability of a chance association is less than 1 percent (Lanza et al. 2011a).

Starspot occultation during planetary transits

- Silva (2003) proposed to use the bumps produced by starspot occultations during transits to map starspots;
- The duration of the bump gives a measure of the spot extension along the transit chord;
- The height of the bump is proportional to the spot contrast.

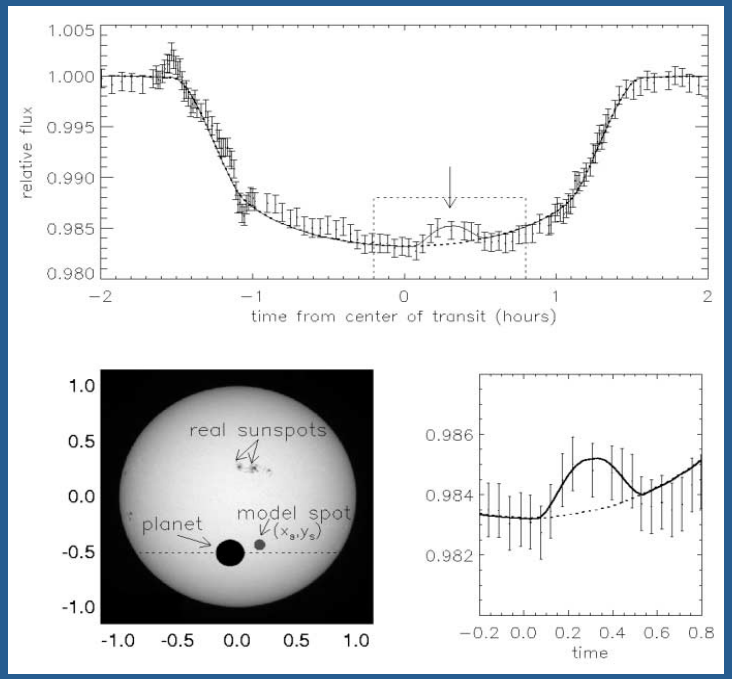

Starspot occultation during transit

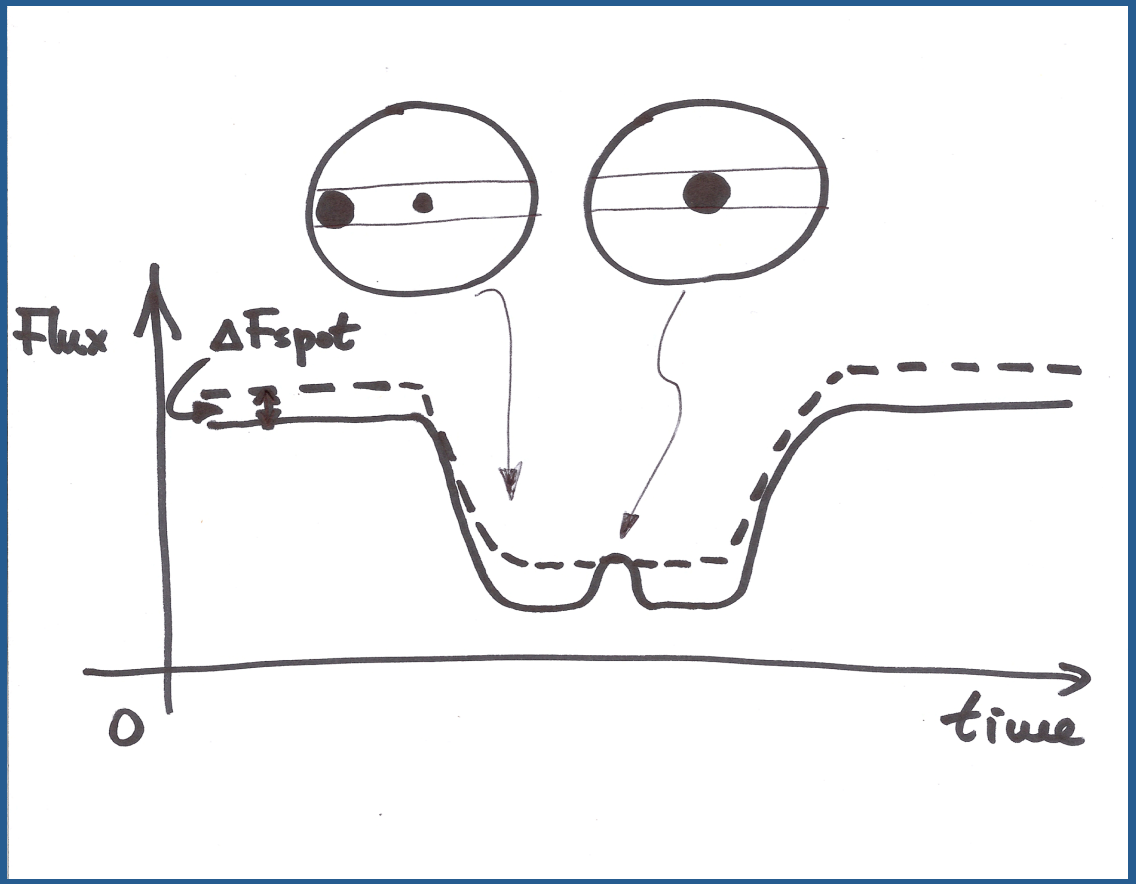

Solid line: transit across the disc of a star with a spot; dashed line: transit in the case of an unspotted star.

Degenerate cases

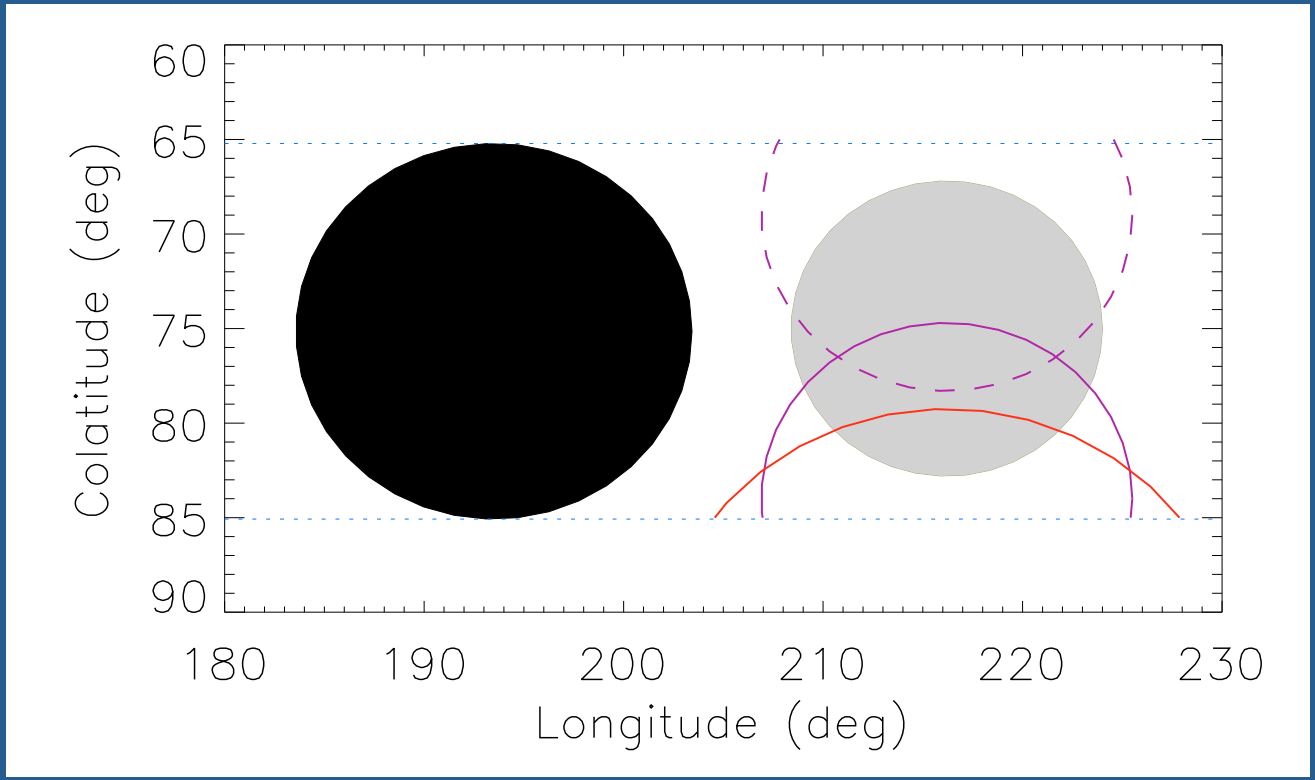

(CoRoT-2: Wolter et al. 2009)

Stellar obliquity and spot occultations

CoRoT-2

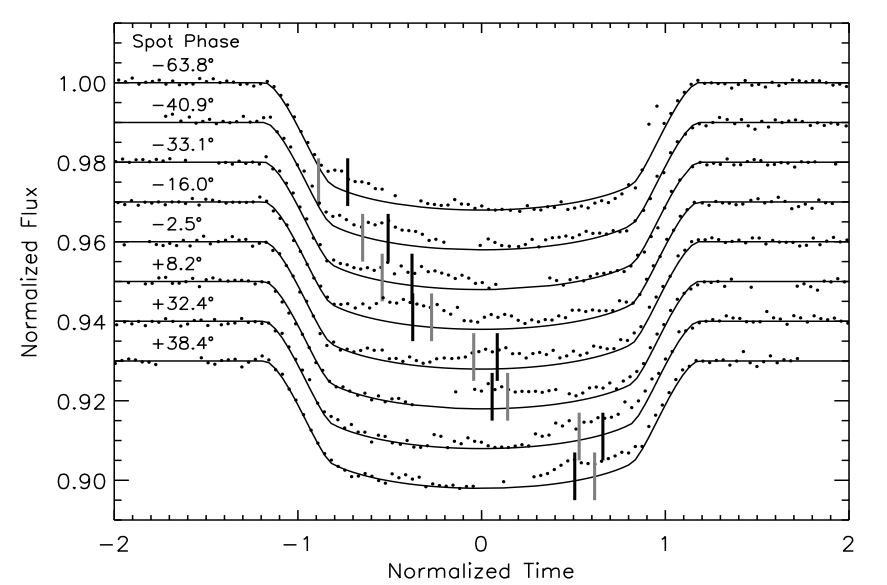

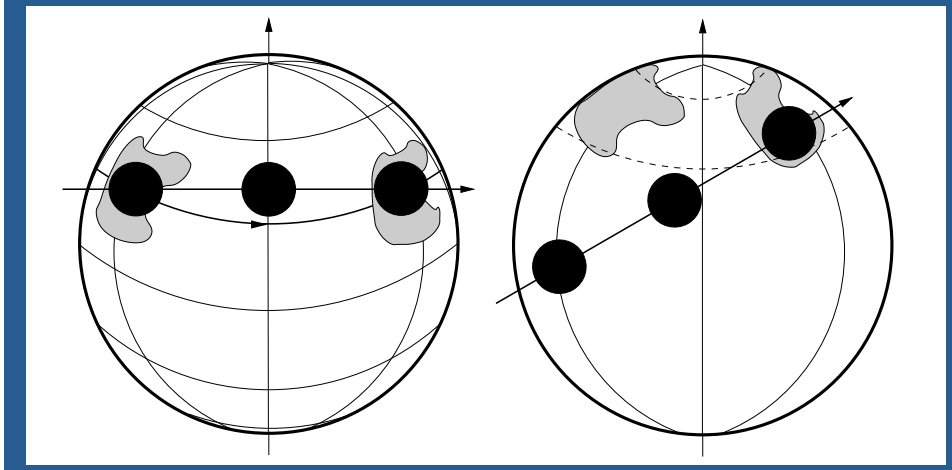

- Nutzman et al. (2011) suggested that if a given spot is repeatedly occulted during successive transits then the projection of the stellar spin axis on the plane of the sky is orthogonal to the transit chord (projected obliquity close to zero);
- Knowledge of the mean spot rotation period is needed to trace the rotation of the spots from one occultation to the next.

An oblique system: HAT-P-11

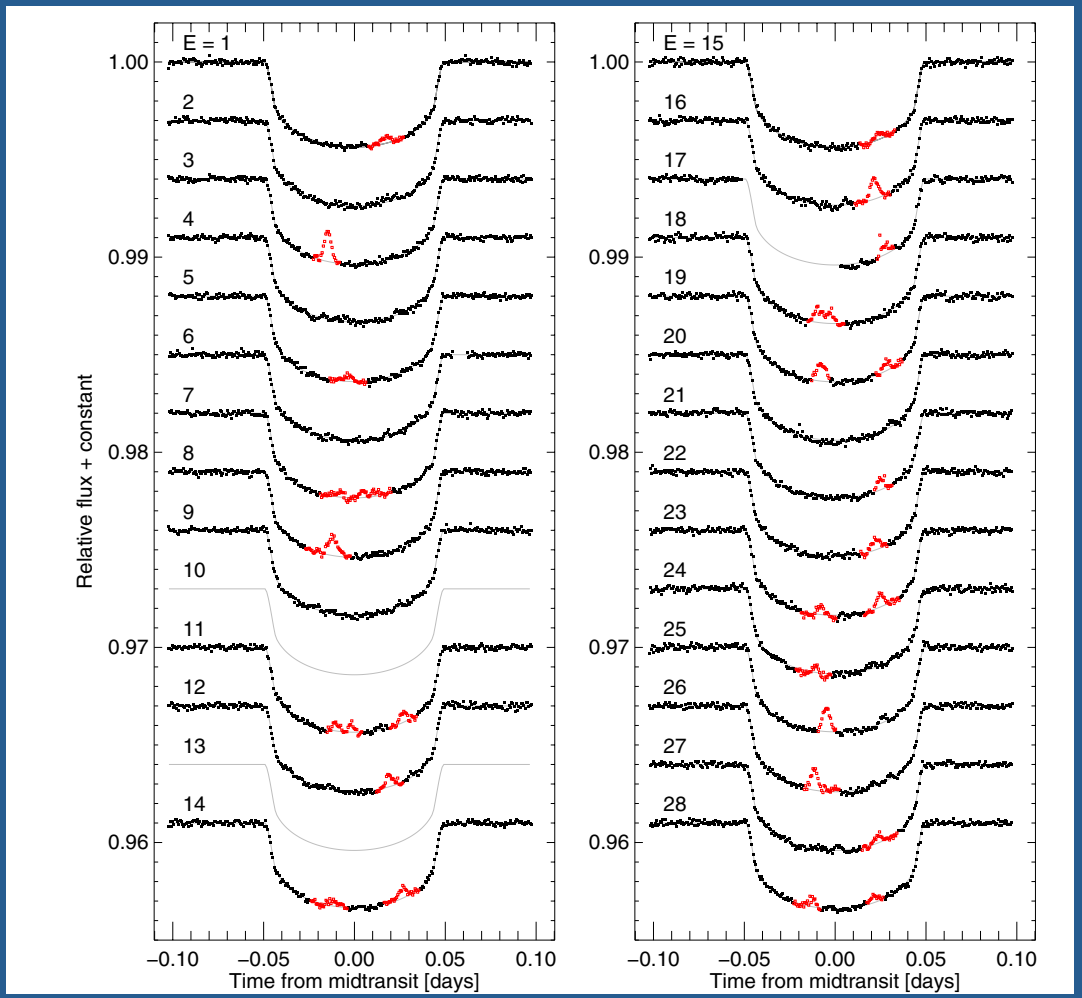

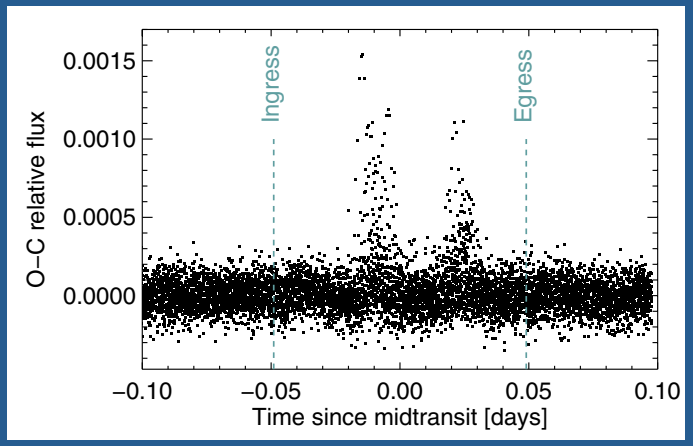

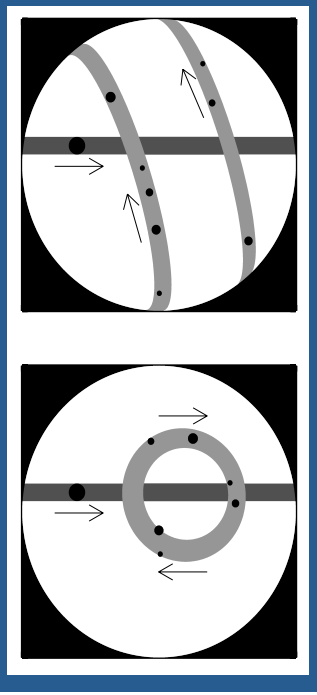

(after Sanchis-Ojeda & Winn 2011; see also Beky et al. 2014)

Starspot properties in CoRoT-2

- Silva-Valio et al. (2010) and Silva-Valio & Lanza (2011) derived longitudes and properties of occulted starspots during 72 transits of CoRoT-2;
- Successive occultations of the same spot along different transits provided information on spot rotation rate at the latitude of the transit chord.

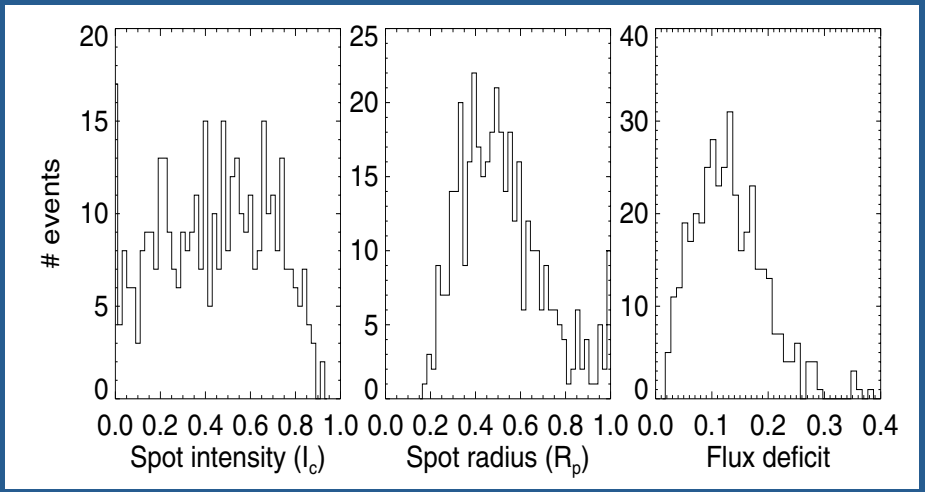

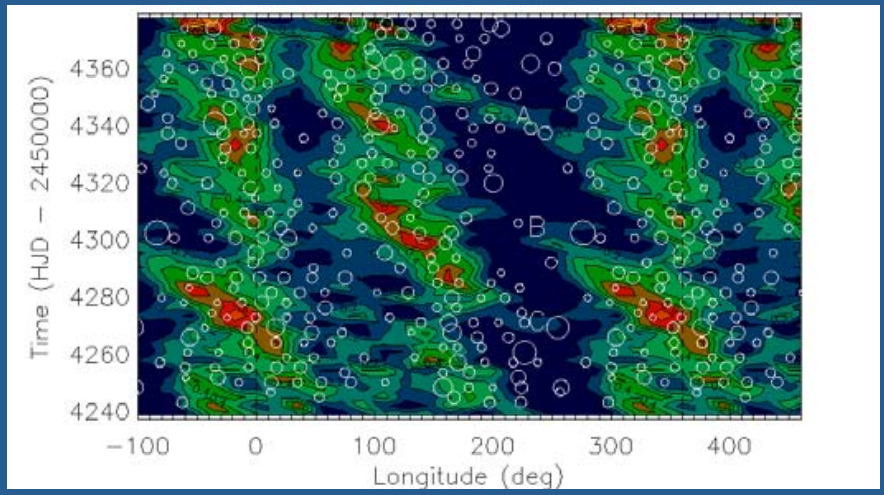

Flux deficit = $(1-I_s) \cdot R_s^2$

The active longitudes mapped from the out-of-transit light curve correspond to concentrations of occulted spots.

Starspot occultations in Kepler-17

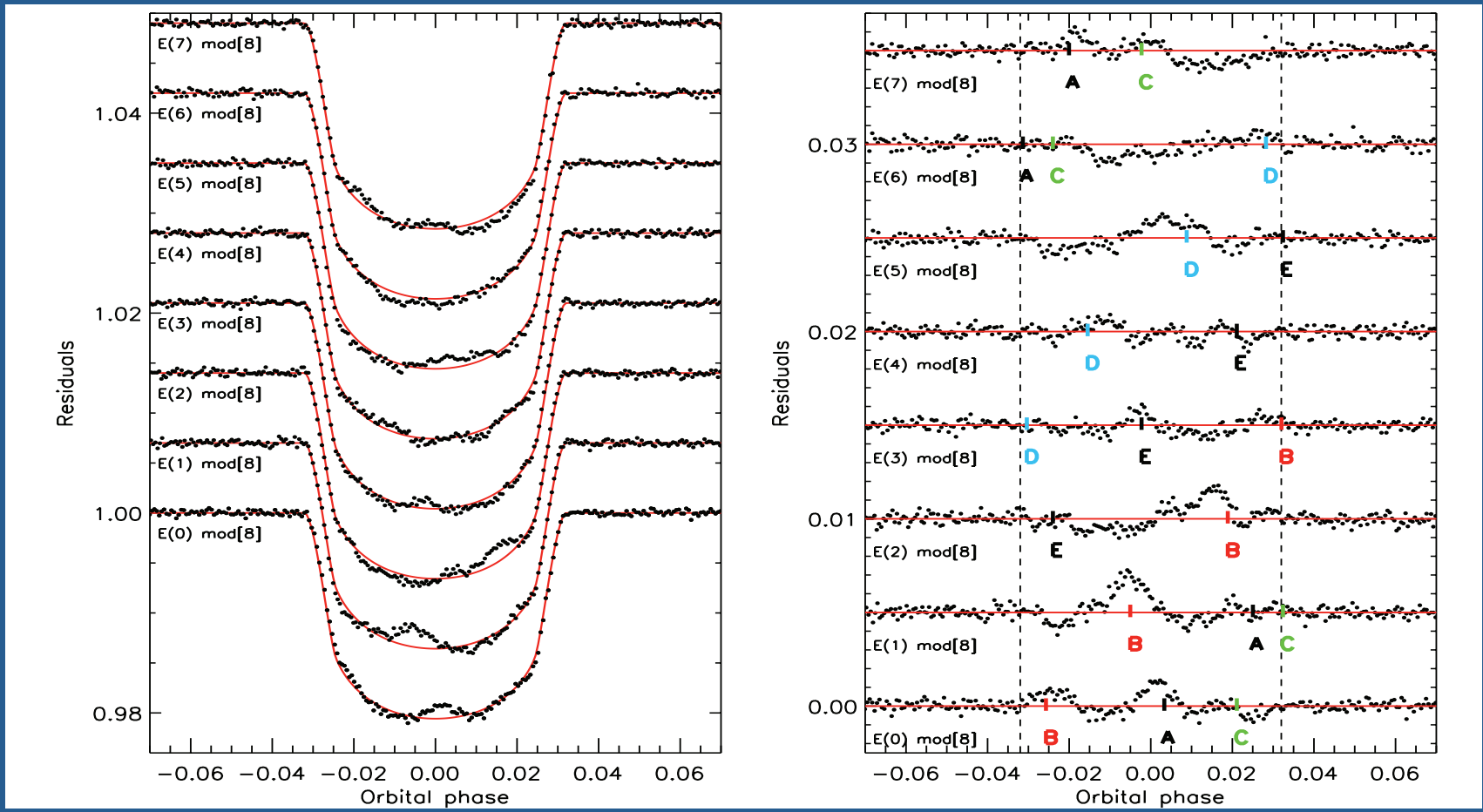

Each co-added transit corresponds to 22 individual transits (Desert et al. 2011).

Spot modelling and the correction of activity-induced RV variations

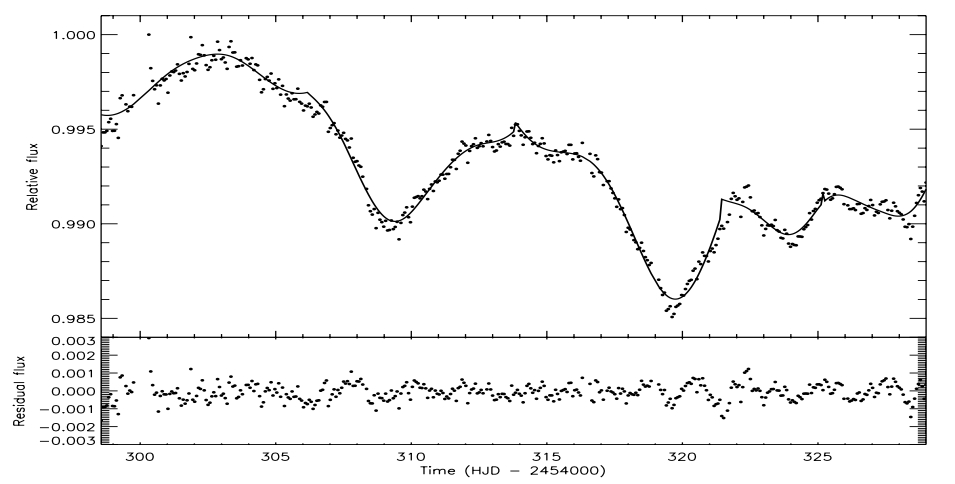

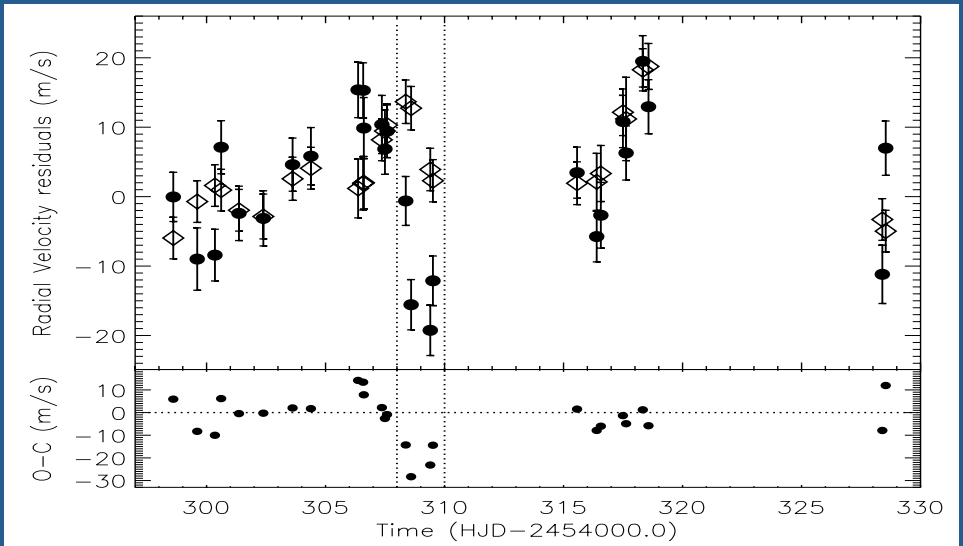

- Lanza et al. (2011b) used MOST photometric observations simultaneous with SOPHIE RV measurements of the active planet-hosting star HD 189733 to model starspot and activity-induced RV variations in that star;
- Some correction of the activity-induced perturbation can be seen in the residuals;
- A simpler approach was proposed by Aigrain et al. (2012);
- They also showed that maps in the photometry nullspace may contribute to the RV variations;
- Therefore, a complete correction may not be possible with this approach, but some improvement is expected (e.g., Meunier & Lagrange 2013).

Conclusions

- Methods for spot modelling based on space-borne high-precision photometry have been reviewed;
- Long-term optical photometric time series acquired to search for planetary transits can be used to study starspot evolution and surface differential rotation (SDR) in late-type main-sequence stars;
- We discussed the results obtained with different modelling approaches as applied to the same dataset, i.e., the light curve of CoRoT-2;
- We derived lower limits to the SDR in four CoRoT targets and in Kepler-17 from the migration of their active longitudes;
- There is evidence of short-term (Rieger-like) spot cycles in CoRoT-2 and Kepler-17;
- Possible magnetic star-planet interaction is suggested in the cases of CoRoT-4 and CoRoT-6, two stars with giant, close-in planets;
- Walker et al. (2008), from MOST observations, found a phenomenology similar to that of CoRoT-4 in τ Bootis; more recently, Beky et al. (2014) provided further indication for HAT-P-11 and Kepler-17.

The end

References

- Aigrain S. et al. 2008, A&A 488, L43
- Aigrain S. et al. 2012, MNRAS 419, 3147
- Alonso R. et al. 2008, A&A 482, L21
- Ballot J. et al. 2006, MNRAS 369, 1281
- Ballot J. et al. 2011, A&A 530, A97
- Barnes J. R. et al 2005, MNRAS 357, L1
- Beky B. et al. 2014, arXiv:1403.7526
- Bonomo A. S., Lanza A. F., 2012, A&A 547, A37
- Bouchy F. et al. 2008, A&A 482, L25
- Berdyugina, S. 2005, LRSP 2, 8
- Collier Cameron A. 1997, MNRAS 287, 556
- Cowan N. B. et al. 2013, MNRAS 434, 2465
- Croll B. 2006, PASP 118, 1351
- Croll B. et al. 2006, ApJ 648, 607
- Cuntz M. et al. 2000, ApJ 533, L151
- Desert J.-M. et al. 2011, ApJS 197, 14
- Donahue R. et al. 1997, Sol. Phys. 171, 191
- Donati, J. F., Collier Cameron A., 1997 MNRAS 291, 1
- Dorren J. D. 1987, ApJ 320, 756
- Eker Z. 1994, ApJ 420, 373
- Frasca A. et al. 2011, A&A 532, A81
- Fröhlich H.-E., 2007, AN 328, 1037
- Fröhlich H.-E. et al. 2009, A&A 506, 263
- Fröhlich H.-E. et al. 2012, A&A 543, A146
- Gizon L., Solanki S. K. 2003, ApJ 589, 1009
- Harmon R. O., Crews L. J. 2000, AJ 120, 3274
- Huber K. F. et al. 2009, A&A 508, 901
- Huber K. F. et al. 2010, A&A 514, A39

- Jetsu L. 1996, A&A 314, 153
- Kollath Z., Olah, K. 2009, A&A 501, 695
- Lanza A. F. 2008, A&A 487, 1163
- Lanza A. F. 2009, A&A 505, 339
- Lanza A. F. 2011, ApSS 336, 303
- Lanza A .F. et al. 1998, A&A 332, 541
- Lanza A. F. et al. 2004, A&A 425, 707
- Lanza A .F. et al. 2007, A&A 464, 741
- Lanza A. F. et al. 2009a, A&A 493, 193
- Lanza A. F. et al. 2009b, A&A 506, 255
- Lanza A. F. et al. 2010, A&A 520, A53
- Lanza A. F. et al. 2011a, A&A 525, A14
- Lanza A. F. et al. 2011b, A&A 533, A44
- Lanza A. F. et al. 2014, A&A 564, A50
- Lehtinen J. et al. 2011, A&A 527, A136
- Lindborg M. et al. 2013, A&A 559, A97
- Lou Y.-Q. 2000, ApJ 540, 1102
- McQuillan A. et al. 2013, MNRAS 432, 1203
- McQuillan A. et al. 2014, APJS 211, 24
- Meunier N., Lagrange A.-M. 2013, A&A 551, A101
- Mosser B., et al. 2009, A&A 506, 245
- Moutou C. et al. 2008, A&A 488, L47
- Nutzman Ph. A. et al. 2011, ApJ 740, L10
- Oliver R. et al. 1998, Nature 394, 552
- O'Neal D. et al. 1996, ApJ 463, 766
- Piskunov N. E. et al. 1990, A&A 230, 363
- Press W. H. al. 2007, Numerical Recipes: the Art of Scientific Computing, Cambridge Univ. Press, Third Edition (http:www.nr.com)
- Reiners A. 2006, A&A 446, 267
- Reinold T. et al. 2013, A&A 560, A4
- Rodonò M. et al. 1986, A&A 165, 135

- Roettenbacher R. M. et al. 2013, ApJ 767, 60
- Sanchis-Ojeda R. Winn J. A. 2011, ApJ 743, 61
- Savanov I. S. 2011, Astron. Rep. 55, 341
- Savanov I. S., Strassmeier K. G. 2005, A&A 444, 931
- Savanov I. S. Strassmeier K. G. 2008, AN 329, 364
- Schneider J. 2000, ASP Conf. Series, vol. 212, p. 284
- Schüssler M., Rempel M. 2005, A&A 441, 337
- Seager S., Mallen-Ornelas G. 2003, ApJ 585, 1038
- Shkolnik E. et al. 2005, ApJ 622, 1075
- Shkolnik E. et al. 2008, ApJ 676, 628
- Silva A. V. R., 2003, ApJ 585, L147
- Silva-Valio A. et al. 2010, A&A 510, A25
- Silva-Valio A., Lanza A. F. 2011, A&A 529, A36
- Strassmeier K. G. 2009, A&Arv 17, 251
- Strassmeier, K. G., 2011, IAU Symp. 273, p. 174
- Vogt S. S. et al. 1987, ApJ 321, 496
- Walker G. et al. 2008, A&A 482, 691
- Walkowicz L., Basri G. 2013, MNRAS 436, 1883
- Wolter U. et al. 2009, A&A 504, 561
- Zappalà R. A., Zuccarello F. 1991, A&A 242, 480
- Zaqarashvili T. et al. 2010, ApJ 709, 749